TEMPERATURE ANALYSIS OF A CLASS OF ELECTROHEATED FLUIDISED BEDS

THESIS

DOCTOR OF PHILOSOPHY

at the

UNIVERSITY OF ASTON IN BIRMINGHAM

by

Ersin Tulunay

September 1969

University of Aston in Birmingham
Electrical Engineering Department

SUMMARY

TEMPERATURE ANALYSIS OF A CLASS OF ELECTROHEATED FLUIDISED BEDS

Fluidisation is an important phenomenon which is used in many chemical and physical processes where heat is a salient factor. In this investigation, practical mathematical models for an important class of electrically-heated fluidised beds have been established. Experimental work was conducted upon laboratory pilot plant and the validity of the derived analytic models has been checked experimentally. These models cater, for the first time, for the (heating and cooling) mode dependence and flow dependence of both directly and indirectly heated fluidised beds. The parameters of these models can be established by a simple series of tests. These models greatly simplify the analysis of existing fluidised bed processes and prediction of the performance of proposed processes.

New flow diagrams were then derived; these give important conceptual insights into the operation of thermal systems. Using these flow diagrams, new steady-state temperature analysis techniques were developed for preheated fluidised beds. These facile techniques greatly simplify temperature analysis within steady-state fluidised beds, and readily evaluate the thermal saving of each stage in a preheated fluidised bed.

ACKNOWLEDGEMENTS

I wish to thank Professor W.K. Roots for his guidance and Professor J.E. Flood for acting as my adviser for the latter portion of the work. I also thank Mr. J.L. Murgatroyd and all members of the research group who encouraged the work and participated in many useful discussions.

I remember my country, Turkey, which prepared me to pursue my studies.

TABLE OF CONTENTS

1 INTRODUCTION

Fluidisation is an important phenomenon which is used in many chemical and physical reactions. The industrial uses of fluidisation; such as chemical manufacture, drying, mixing, materials handling and many others, continue to increase promisingly. Extensive work has been conducted on both scientific and applications aspects of this subject and these results are contained in the literature. General information about the published works can be found in the survey reports[1,2].

In many chemical and physical reactions, heat is an important factor, and the state of the output product is significantly dependent on the processes' thermal conditions. Therefore, a powerful temperature analysis technique is necessary for the process to achieve the desired result. Although a considerable amount of work has been undertaken on basic phenomena within these beds, such as heat or mass transfer mechanisms, insufficient consideration has been paid to the entire bed system. There are no complete mathematical models which represent the electrically-heated fluidised beds and which can be used to study temperature-control strategies. In this investigation, mathematical yet practical models for an important class of electrically heated fluidised beds have been derived.

Experimental work was conducted using laboratory pilot plant and the validity of the derived analytic models was checked experimentally. These new analytic models are complete in that they consider both the flow-dependence and the heating and cooling mode-dependence of this system.

A new flow-diagram technique has been developed as a practical tool that considerably simplifies the analysis of steady-state temperatures and related phenomena in thermal processes involving a plurality of heat exchanges. This is further developed to provide a new approach for quickly analysing the effects of preheating in fluidised bed systems. These new flow-diagram techniques are used in this study and, although fluidised beds are primarily studied, these techniques are equally applicable to other thermal processes involving a plurality of heat exchanges between two materials.

2 HEATING IN FLUIDISED BEDS

Fluidised beds are beds of particulate matter through which a fluid (gas or liquid) flows. At a critical velocity of fluid flow through the bed, and a corresponding critical pressure drop across the bed, the particulate matter no longer behaves as a solid mass, but behaves like a fluid; i.e. fluidisation of the bed has occurred. Fluidisation has been described in the literature and general information can be found in the references cited; 3, 4 and 5. In the literature describing the fluidised beds the terms "fixed" and "moving" beds are often used to describe the states of operation. A fixed bed would be a motionless mass of particles before fluidisation (i.e. supported by contact with each other). After fluidisation, these particles remain in mutual contact but the entire bed moves with respect to the walls of the containing vessel (i.e. a moving bed).

For the ideal case, the fixed pressure drop ΔP across a packed bed of particles increases with increasing fluid flow. When the pressure drop equals the "weight loading per unit base area of the bed", then fluidisation has occurred and the pressure drop remains constant, independent of flow rate. The flow, f_o, at which fluidisation occurs, and the corresponding velocity are called the "minimum fluidising flow rate" and the

"minimum fluidisation velocity" respectively. The relationship between the pressure drop Δp and the fluid flow f is shown in Fig. 2.1 (experimental curve is in Fig. A-1).

FIG. 2.1

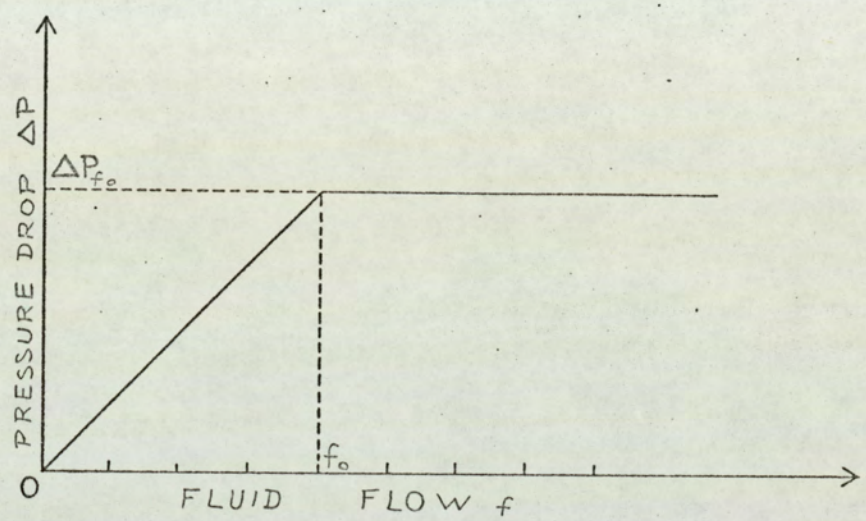

FIG. 2-1. Pressure-Drop fluid-flow relationship in the bed.

In this study, the minimum fluidising flow rate f_o was determined by observing the pressure drop using a water manometer. Although an alternative method has recently been suggested[6], the pressure-drop method was found to be more suitable for the class of system under investigation.

In this study, two kinds of electric heating are used. "Indirect-electroheated" (or "indirectly electrically heated") beds are heated by electrical elements inserted in the fluid flow before the bed. On the other hand, a fluidised bed of conducting particles can be heated by

passing a current through electrodes immersed in the bed. The electrical resistance of the bed converts electrical energy directly into heat. Such beds are described as "direct-electroheated" (or "directly electrically heated") fluidised beds.

The experimental procedures are described in the following two chapters. A full account of the experimental work is given in Appendix A.

3
INDIRECT - ELECTROHEATED FLUIDISED BEDS

3.1. Introduction

In this chapter the above class of fluidised beds is investigated. These are indirectly heated by electrical elements inserted in the fluid flow before the bed. The term "bed" identifies the particulate mass, its container, and its porous supporting layer. The beds were of circular cross-section with a fixed-bed height of the same order as the radius of the containing vessel. The term "heater" will refer to both the heating element and its surrounding air stream. This convention has advantages. Firstly, it caters for the "flow-dependence" of the heater parameters. Secondly, while this study is essentially interested in an application of electroheat, the results can be applied to non-electric forms of heating. The term "system" refers to the combination of the heater and the bed. In the laboratory models the bed was readily detachable from its heater. A "dummy" bed, which had the same fluid - flow impedance as the actual bed, but lacked its coupled time constant, was also used. Thus, studies of a heater and a "dummy" bed determined the heating performance of the heater. Also, when a heater and dummy bed were brought up to a steady state, the dummy bed could be exchanged for a real bed in negligible time; which readily permitted observation of the

FIG. 3-1

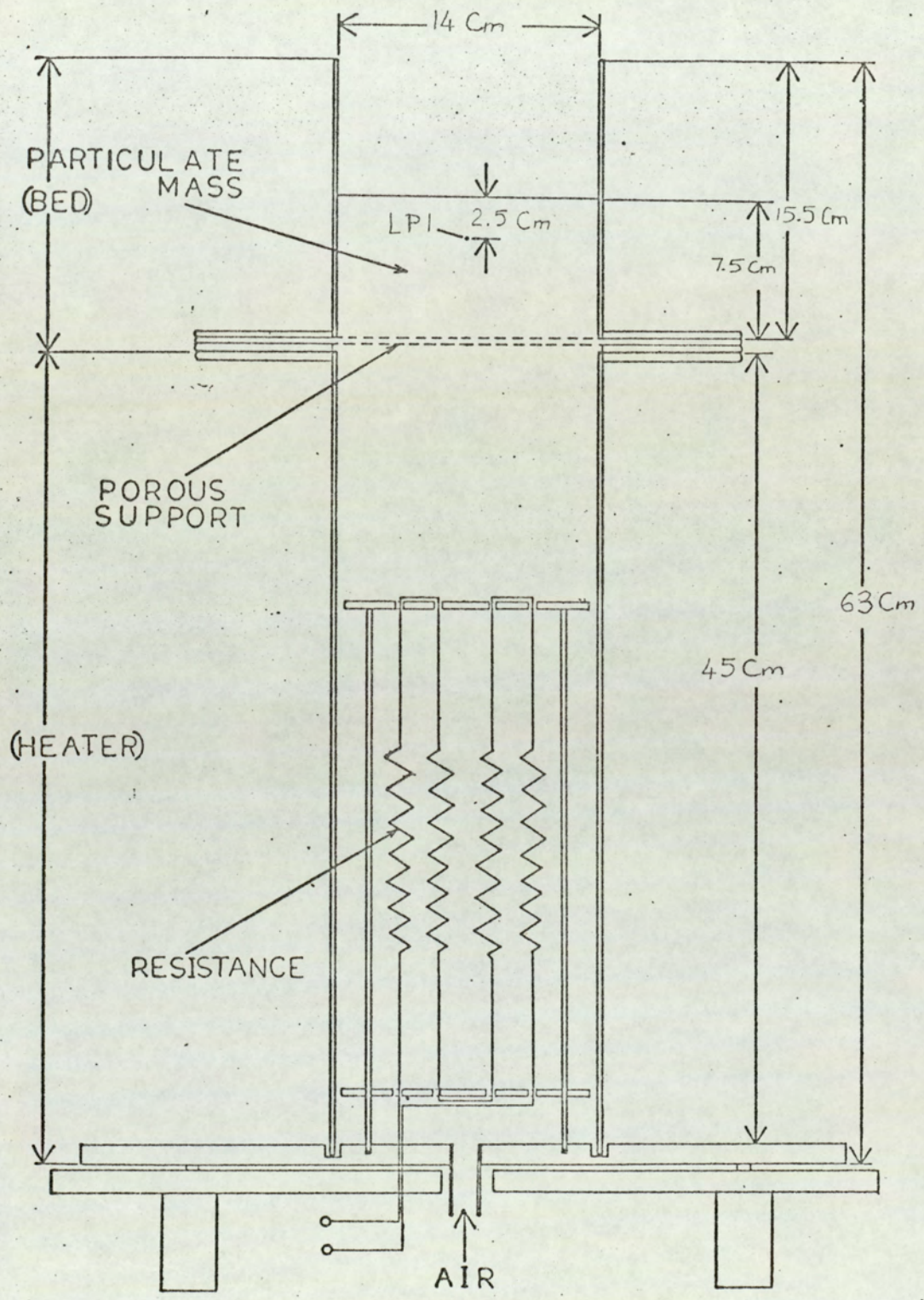

FIG. 3-1: Typical Model of the class of bed studied.

heating performance of the bed alone. For cooling tests, a steady-state heated bed was transformed to a "dummy" heater, which had the fluid-flow impedance of a heater, but lacked the thermal input. This permitted determination of the cooling properties of the bed alone. To determine the cooling properties of the heater alone, the heater cooled while coupled to a dummy bed. A typical laboratory model is shown in Fig. 3-1. The l.p.i. (location of particular importance) in the bed was taken as location (L.P.I.) in Fig. 3-1. This is the centre of the circular cross-section and about one third of the fixed-bed height below the surface which is reasonably free from side effects. It is also a common exit temperature point when the particulate matter flows continuously. However, the results would be applicable to any other l.p.i. s that gave similar responses to those to be displayed.

Most of the beds investigated used around 60 mesh SiC, but tests with other materials, coke , etc., showed that the analytic model was generally applicable provided the appropriate characteristics were inserted (see Figs. A-2 – A-5).

3.2. Heating model

The normal operation region of this class of bed is defined as

$$f_o \lesssim f \lesssim f_2 \qquad (3\text{-}1)$$

where f = flow at the operation point
f_o = minimum fluidising flow
f_2 = upper limit flow in practice
} (m^3/hr); (ft^3/hr)

A "very high flow rate", f_3, is also used to determine some characteristics of the bed. The flow rates f_o, f_2 and f_3, ($f_o < f_2 < f_3$) are determined according to the nature of the bed, and their numerical values do not restrict the generality of the results.

After examining the heating response of the system to a step input of electrical power, a third-order model with transit delay was established for the system at $f = f_o$ by curve fitting (see Fig.A-3). The response to unit step of electrical power in s domain is

$$\theta(s) = \frac{G \exp(-sL_o)}{(1+s\tau_{ho})(1+s\tau_{bo})(1+s\tau_{b3})} \qquad (3\text{-}2)$$

where G = the system gain, i.e.: maximum temperature for selected heater (^oC); (^oF)

τ_{ho} = the heater time constant at $f = f_o$ which is determined by using the dummy bed at the top of the heater (sec) (see Fig. A-4)

τ_{bo} = the characteristic time of the bed when $f = f_o$ (sec)

τ_{b3} = the characteristic time of the bed when $f = f_3$ (sec)

L_o = the transit delay at $f = f_o$ (sec) which is determined from the system heating response at $f = f_o$

At very high flow, f_3, it was found that the heating response was a first-order curve (Fig.A-3). By using the heating response of the system which is recorded at $f = f_3$ the time constant τ_{s3} and hence τ_{b3} is found

$$\tau_{b3} = \tau_{s3} - \tau_{ho} \qquad (3\text{-}3)$$

A response time τ_s, for the higher order system, is defined as the time taken for the system heating response to rise from 0.05% to 63.5% of its final steady state value. From the heating response of the system at $f = f_o$, the response time τ_{so} is calculated. Then by Eq. (3-4), τ_{bo} is determined.

$$\tau_{bo} = \tau_{so} - \tau_{ho} - \tau_{b3} \qquad (3\text{-}4)$$

From a typical heating curve at $f = f_o$, system gain G is also determined. In Figs. 3-2. and 3-3, typical heating response of the system and model, and initial portions of these curves are shown respectively.

FIG. 3-2

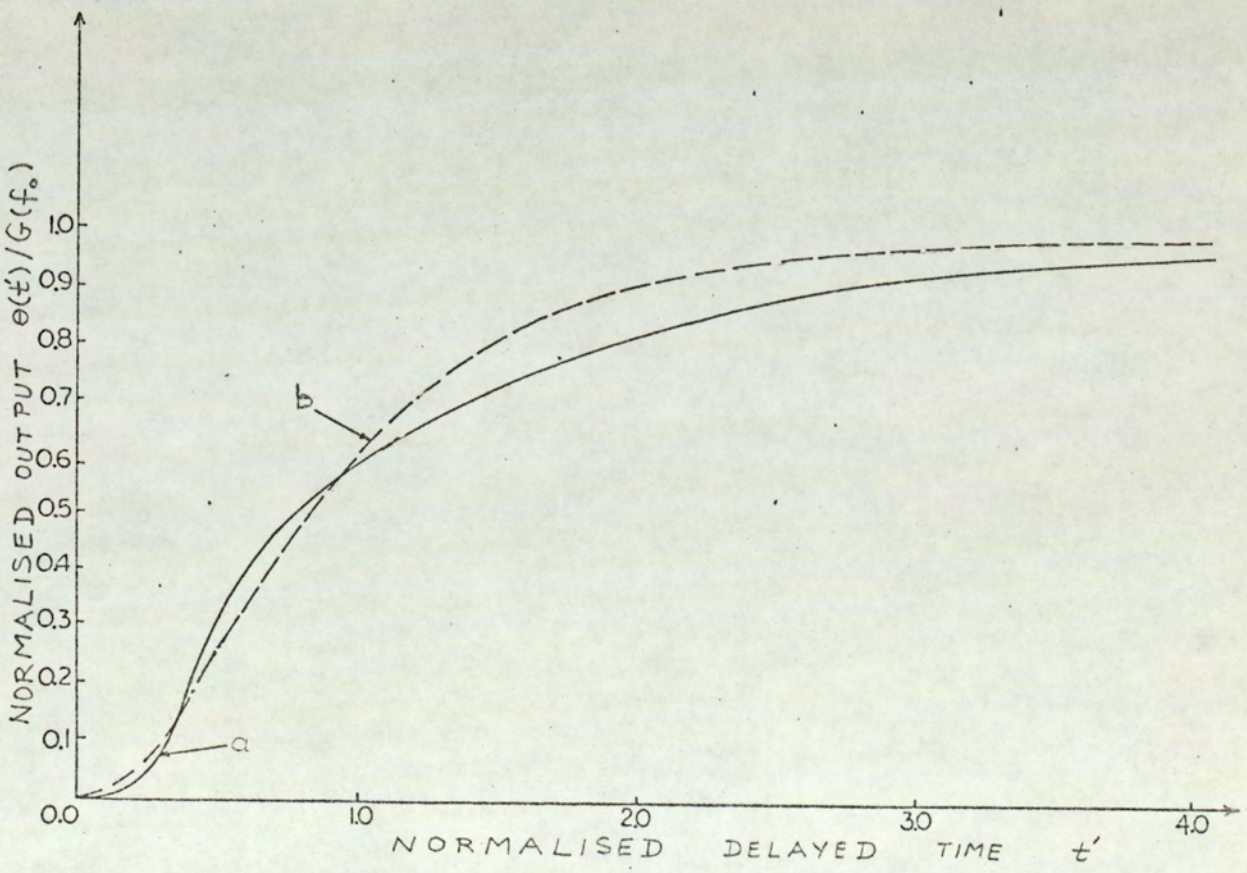

FIG. 3-2: Typical heating response of (a) system (see also Fig.A-2) and (b) model

FIG. 3-3

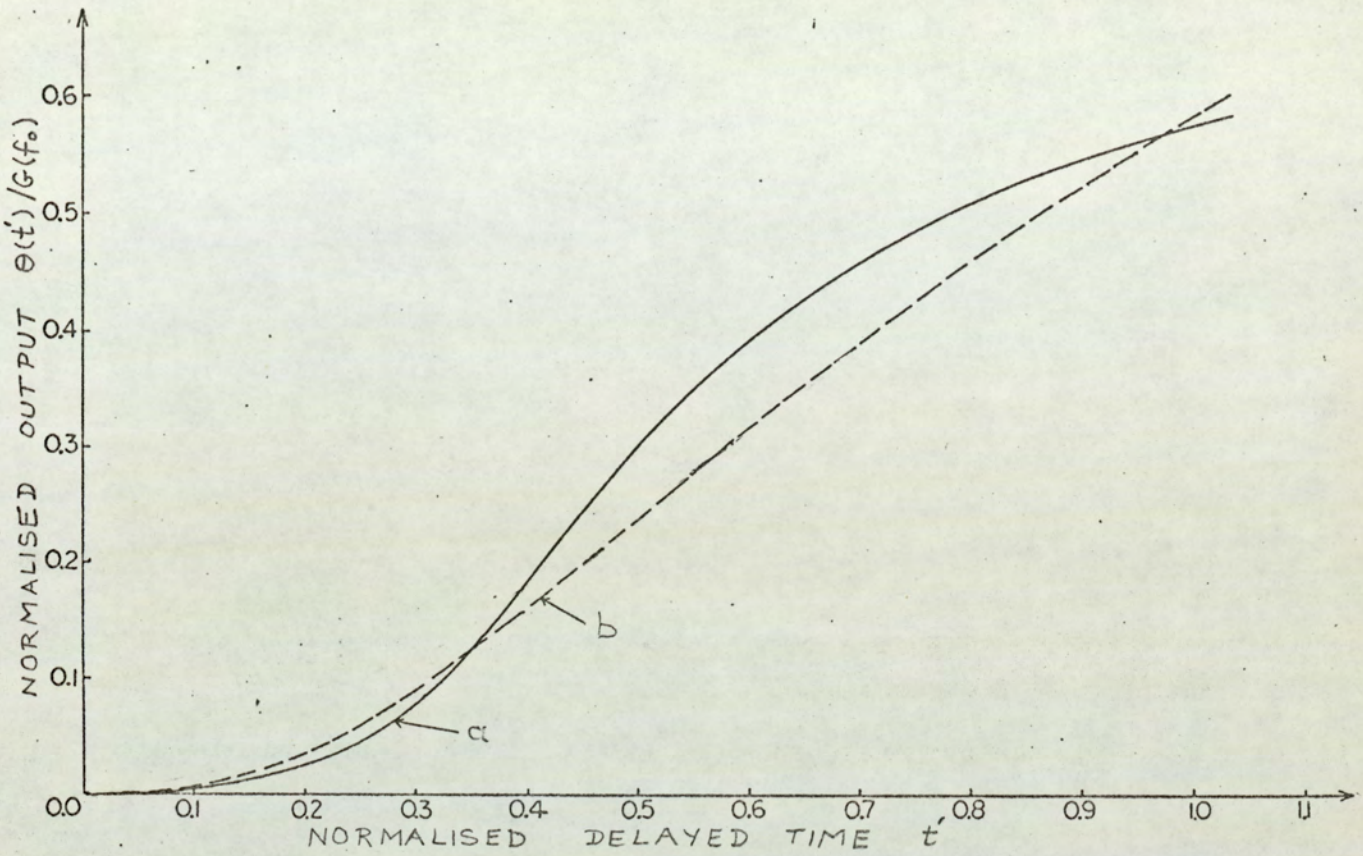

FIG. 3-3: Initial portion of (a) system and (b) model response in Fig. 3-2.

The change of bed parameters with the varying flow rates was determined by performing other tests at intermediate flow rates. It was established, experimentally, that the heater time constant τ_h and the system response time τ_s are flow dependent, and that this flow dependence is approximately linear in the normal operating region defined in Eq. (3-1). For simplicity, the flow dependencies of the time constants and response times were included in the heater time constant. Thus, a "heater equivalent time constant " $\tau_{he}(f)$ is defined as a linearly-decreasing

function of flow, while τ_{bo} and τ_{b3} are taken to be constant.

The transit delay L(f) was also found to be a linear decreasing function of flow. This is shown in Fig. 3-4 (see also Figs.A-2, A-3).

FIG. 3-4

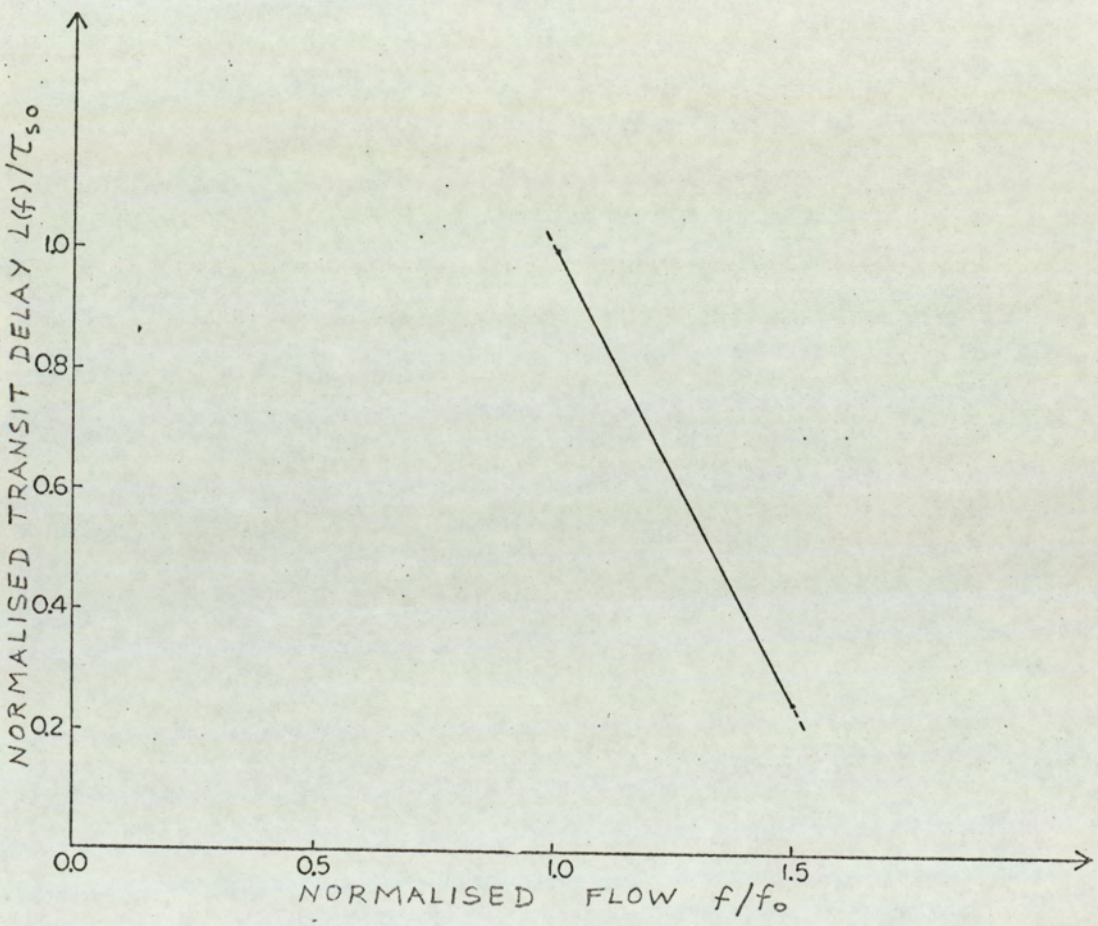

FIG. 3-4: Typical flow dependence of transit delay.

Thus, the flow dependent model is

$$\frac{G(f)\ [\exp\ -s\ L(f)]}{[1+s\ \tau_{he}(f)]\ (1+s\ \tau_{bo})\ (1+s\ \tau_{b3})} \qquad (3\text{-}5)$$

Normalised displays of the system gain as a function of flow (for constant electric power input) and the electric power input as a function of flow (for constant gain) are shown in Fig. 3-5 as lines (a) and (b) respectively (see also Figs. A-2,A-3).

FIG. 3-5

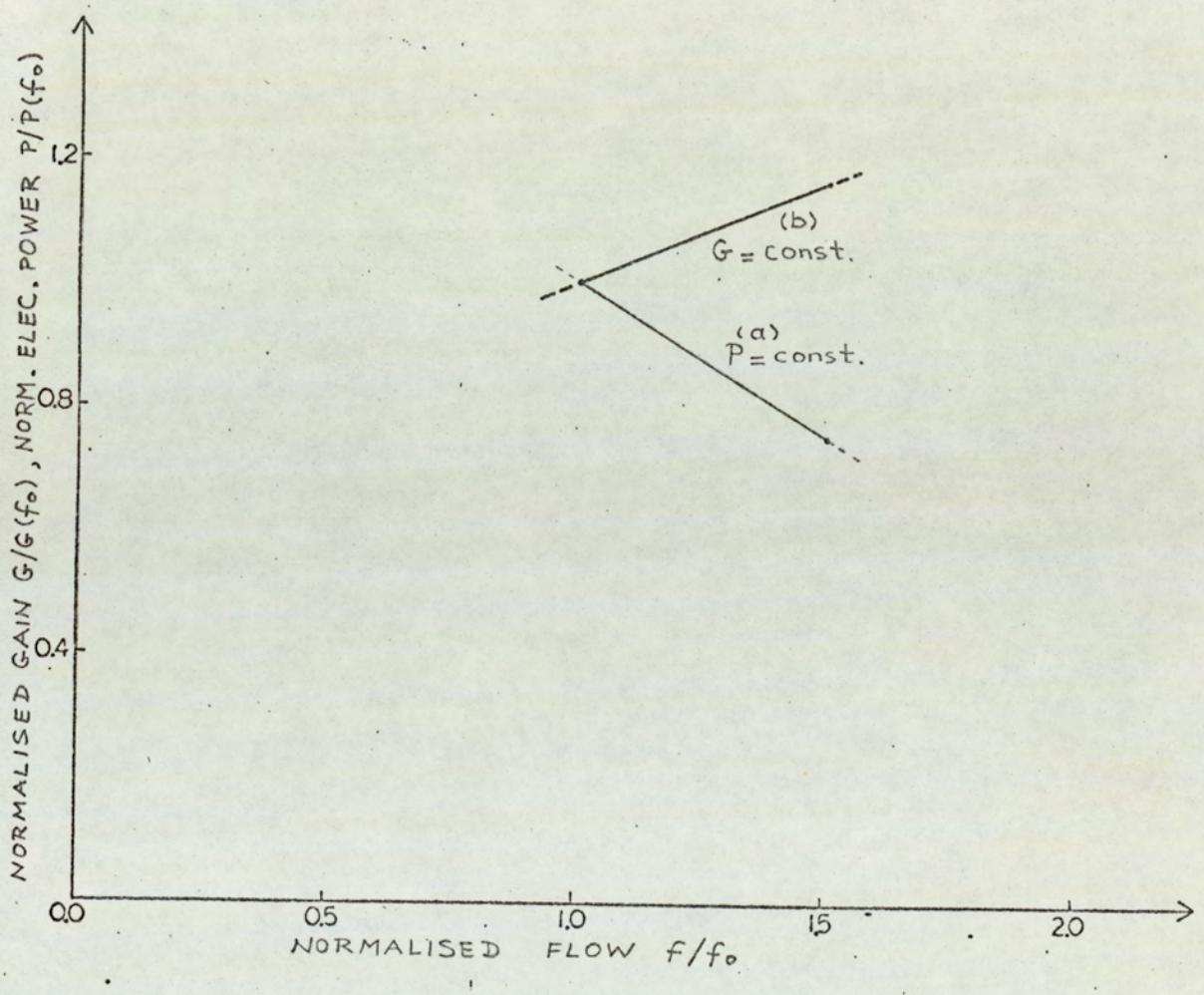

FIG. 3-5: Typical flow dependence of (a) system gain and (b) electrical power input.

3.3 Cooling model.

The response of the system in the passive mode, cooling, was found to be a first-order delayed response of the form

$$\theta_c(t,f_c) = \theta(0) + \theta(t_{ic}) \exp\left[-\frac{t - L(f_c)}{\tau_{sc}}\right] \quad (3\text{-}6)$$

(see Figs. A-1,A-2 and A-3)

where θ_c = cooling response (^oC); (^oF)

f_c = flow at cooling (m^3/hr); (ft^3/hr)

t_{ic} = time at which cooling begins (sec)

τ_{sc} = system cooling time constant (sec)

τ_{sc} is found to be reasonably linear over the normal operation range,which is displayed together with system heating response time τ_s in Fig. 3-6 (see also Figs. A-2,A-3).

Cooling response in s domain is

$$\Theta_c(s,f_c) = \theta(0) + \theta(t_{ic}) \frac{\left[\exp - sL(f_c)\right]}{(1 + s\tau_{sc})} \quad (3\text{-}7)$$

3.4 Conclusions

(a) For a class of indirectly electrically heated fluidised beds, new models have been developed for heating and cooling.

(b) These models involve only tests on the heater and the bed assembly. They do not involve tests on the bed components: material, container, porous support, etc.

FIG. 3-6

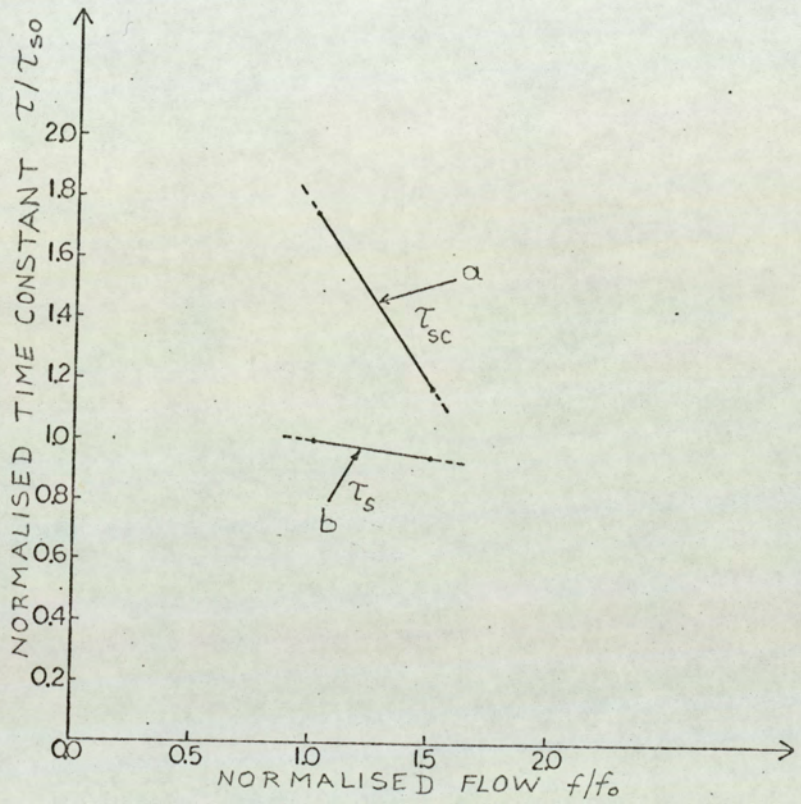

FIG. 3-6: Typical flow dependence of cooling time constant with heating response time shown for comparison.

(c) The models involve tests at only three flow rates, the minimum fluidising flow f_o, the upper limit flow f_2, and very high flow f_3.

(d) An important result of this investigation was the heating model in which the bed time constants appeared as low flow f_o and very high flow f_3 components. This model was extended to be flow dependent.

4 DIRECT-ELECTROHEATED FLUIDISED BEDS

4.1. Introduction

A class of conducting fluidised beds was studied. New models have been developed which are complete and can readily be determined from a simple test series.

The literature contains some reports on the electrical properties of fluidised beds. The electrical resistance of fluidised beds will be briefly surveyed in Section 4.5. Electrostatic phenomena in fluidised beds have been reported[7,8]. The electrical characteristics of the beds have been used to investigate some of their important properties[9,13]. Industrial-process applications and temperature-control aspects[14] have been reported, as well as design considerations and voltage/current relationships[15].

Although some work has been undertaken on the individual electrical characteristics of the conducting beds, insufficient consideration has been paid hitherto to the entire bed system. In this chapter, previous models are considered and simplified to make them easier to handle. Flow dependence of parameters is introduced to derive complete, practical models of these beds in their heating and cooling modes.

In this chapter the term "bed" continues to identify the particulate mass, its container and its porous supporting layer; while the term "system" now identifies the combination of bed and electrodes. The beds were of circular cross-section with a fixed-bed height of the same order as the radius of the containing vessel. However, the findings can be applied to beds with other height/radius ratios, provided that the system response is of the same general form as the responses studied.

The beds studied were energised by alternating current, and coke particles of around 60 mesh were used as the solid medium in the bed.

The l.p.i. (location of particular importance), at which temperature is controlled, was typically as location 1 of Fig. 4.1 which shows a typical laboratory model of the class of bed investigated.

FIG. 4-1

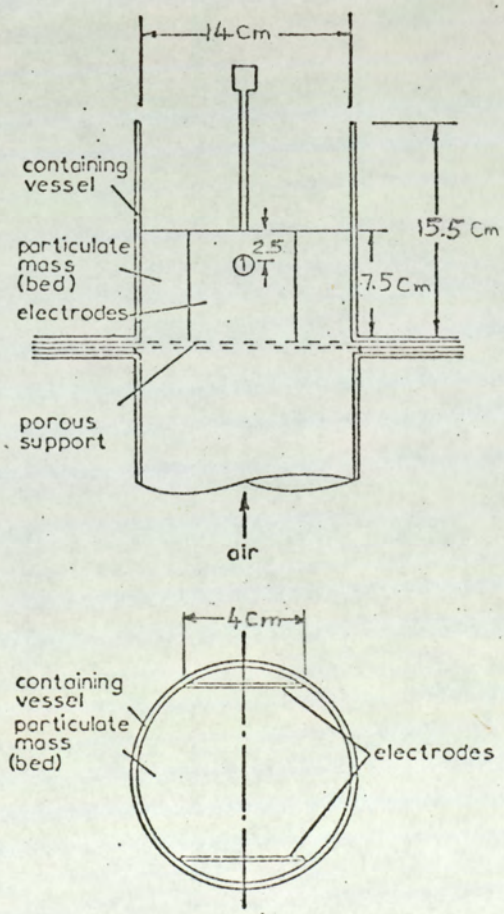

FIG. 4-1: Typical laboratory model of the class of bed studied,
a) front view
b) containing-vessel top view

The normal operating range of the beds studied was

$$f_o \leq f \leq 1.4\ f_o \qquad (4\text{-}1)$$

However, some experiments were carried out also beyond this range. It should be noted that expression (4-1) does not restrict the generality of the results obtained; the ratio may be greater in other processes as a result of the construction.

In this investigation, four principal types of experiment were conducted:

(a) By adjustment of the electrical-power input, the maximum temperature at the l.p.i., i.e. the system gain, was maintained constant for various flows.

(b) The electrical-power input was held constant while the flow varied.

(c) When the system was in the steady state at maximum gain, i.e. at maximum l.p.i. temperature, the power was disconnected and the system allowed to cool.

(d) The bed resistance was measured at varying flow rates.

4.2. Heating

The basic nonlinear differential equation which relates the bed temperature to other parameters, described in recent literature[16], has been simplified and solved. Flow dependence, which was ignored by previous workers in the field, has now been included and the complete solution has been established. The following subsections give an outline of the work involved.

4.2.1. The basic differential equation

The differential equation giving the bed temperature during heating has been found to be[16]

$$\Sigma m_i c_i \frac{d[\theta(t)]}{dt} + K\left[\theta(t)\right].B.\left[\theta(t) - \theta(0)\right] = Q \quad (4\text{-}2)$$

where t = elapsed time (since switch on) (sec)

$\theta(t)$ = temperature at l.p.i. (^{o}C); (^{o}F)

$\theta(0)$ = $\theta(t)$ at $t = 0$ (^{o}C); (^{o}F)

m_i = mass (kg); (lb)

c_i = specific heat (J/kg ^{o}C); (Btu/lb ^{o}F)

$K\left[\theta(t)\right]$ = combined coefficient of heat emission per unit of surface area, time, and temperature ($J/hr.m^2.{}^{o}C$): ($Btu/hr.ft^2.{}^{o}F$)

B = lateral surface area of the apparatus (m^2), (ft^2)

Q = heat energy per unit time (J/hr); (Btu/hr)

$\Sigma m_i c_i$ represents the amount of heat absorbed by the solid particles, bed walls, electrodes, porous plate, etc. $K\left[\theta(t)\right].B$ is the heat absorbed by the fluidising gas and the environment. $K\left[\theta(t)\right]$ was represented as

$$K\left[\theta(t)\right] = a\theta(t) + b \quad (4\text{-}3)$$

where a = constant to represent the temperature-dependent heat emission ($J/hr.m^2.{}^{o}C.{}^{o}C$); ($Btu/hr.ft^2.{}^{o}F.{}^{o}F$)

b = constant to represent the temperature-independent heat emission ($J/hr.m^2.{}^{o}C$); ($Btu/hr.ft^2.{}^{o}F$)

The solution of Eq. (4-2) is[16]

$$\frac{\sqrt{a}\theta(t) + D - Z}{\sqrt{a}\theta(t) + D + Z} \cdot \frac{\sqrt{a}\theta(0) + D + Z}{\sqrt{a}\theta(0) + F - Z} = \exp\left(-\frac{B\sqrt{a}}{\Sigma m_i c_i}\right) Zt \qquad (4-4)$$

$$\text{where} \quad D = \frac{b - a\theta(0)}{2a}$$

$$Z = \sqrt{\left(\frac{b + a\theta(0)}{2a}\right)^2 + \frac{Q}{B}} \qquad (4-5)$$

Using typical values and taking $\theta(0) = 0$ we can display the curve corresponding to Eq. (4-4) as curve a in Fig. 4-2. This is similar to a first-order step response. In fact, if the temperature dependence of $K[\theta(t)]$ is ignored (i.e. $a = 0$) the solution of Eq. (4-2) yields a first order $\theta(t)$ response with a time constant

$$\frac{\Sigma m_i c_i}{b} \qquad \text{(see curve b of Fig. 4-2)}$$

Normally $a \ll b$. Therefore, disregarding a does not make a significant change in the general shape of $\theta(t)$. But, with the same parameters, a first-order response will be faster as is seen in curve b of Fig. 4-2. Thus, a modified time constant must be found.

We define a response time τ_1 for the exact $\theta(t)$ response (curve α, Fig. 4-2) as the time required by $\theta(t)$ to reach 0.632 of its final value. If a first-order response is plotted using τ_1, it will still be faster initially (curve c, Fig. 4-2). A new, modified, time constant τ_{1n} must be used with the first-order response to get a better approximation to the actual response (curve a, Fig. 4-2).

τ_{1n} can be determined by trial and error, or can be established experimentally in a manner to be described later. In Fig. 4-3, curves a, b and c are, respectively, the responses of the actual system, a first order system with time constant τ_{1n} and a first-order system with time constant τ_1; they are all displayed on enlarged scales.

FIG. 4-2

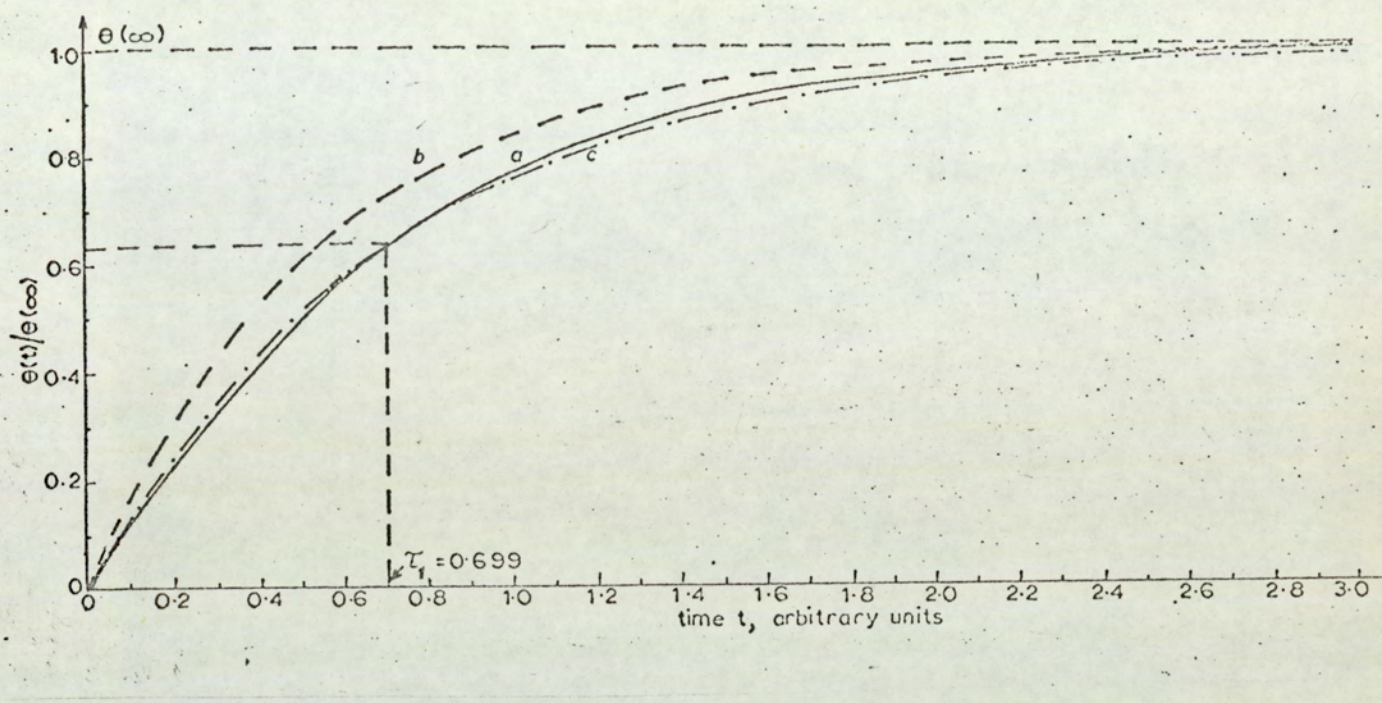

FIG. 4-2: Curve for Eq. 4-4

(a) actual system
(b) curve for a = 0
(c) curve of 1-exp (-t/0.699)

Generally, in industrial-control applications, only relatively small temperature changes are permitted at the l.p.i. Then, the temperature-dependent heat emission, $a\theta(t)$ in Eq. (4-3) does not change significantly. This is another justification for the disregard of the temperature dependence of the heat emission.

FIG. 4-3

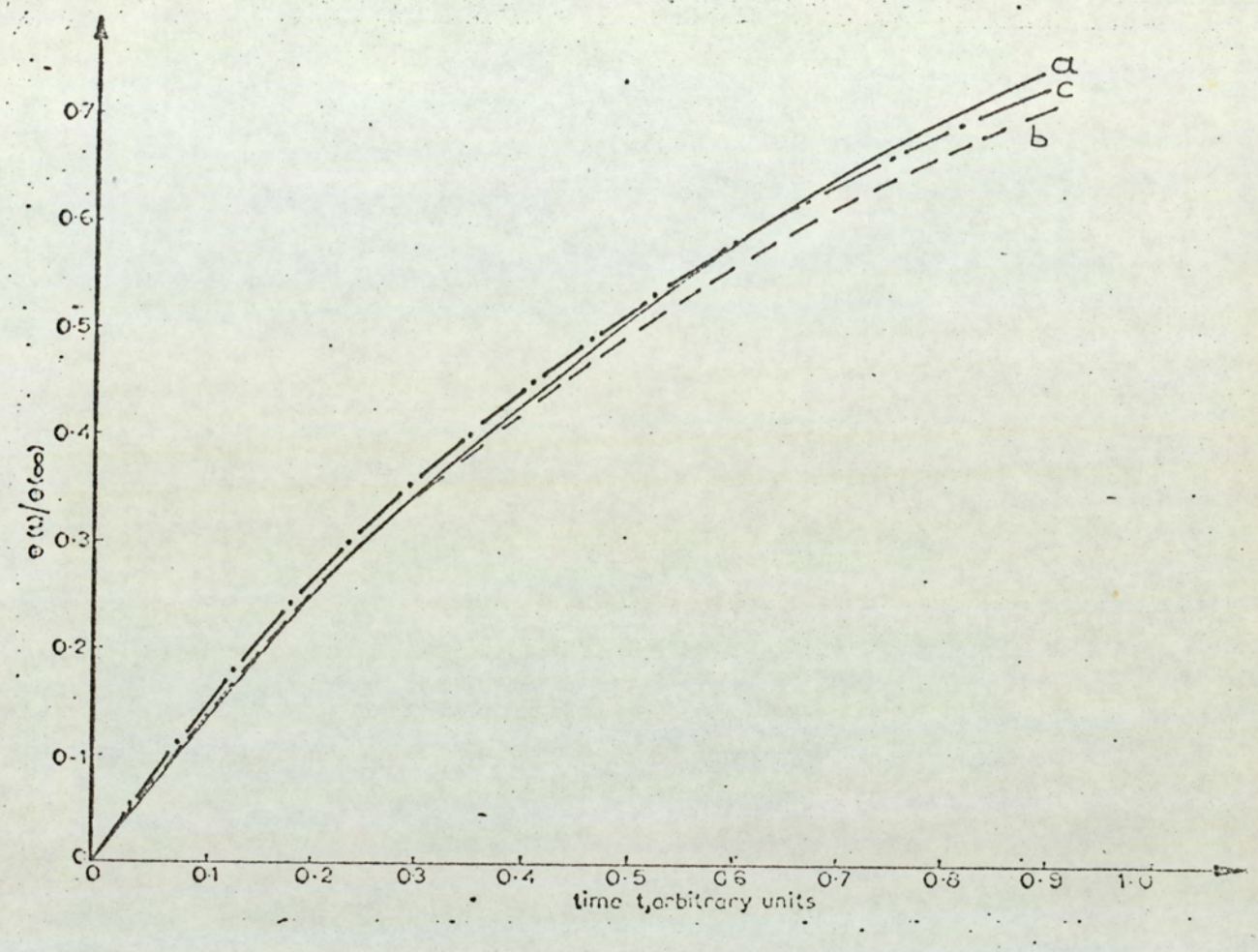

FIG. 4-3: Enlargement of the initial portion of the curve for Eq. 4-4

(a) actual system
(b) first-order curve with the new modified time constant, τ_{1n}
(c) first order curve with the modified time constant, τ_1

4.2.2. A simpler first-order model

For the temperature-independent heat emission the differential equation for heating is

$$\Sigma m_i c_i \cdot \frac{d\,\theta(t)}{dt} + \beta\left[\theta(t) - \theta(0)\right] = Q \qquad (4\text{-}6)$$

where β = Temperature-independent coefficient of heat emission to the environment and fluidising gas in heating ($J/hr^{\circ}C$); ($Btu/hr^{\circ}F$)

The solution to this equation is

$$\theta(t) = \theta(0) + \frac{Q}{\beta}\left[1 - \exp\left(-\frac{\beta}{\Sigma m_i C_i}\right) t\right] \quad (4\text{-}7)$$

The heat-emission coefficient β in Eq. (4-6) must have a flow-dependent component, because it represents the amount of heat absorbed by the environment and by the fluid. The magnitude of the flow-dependent component will vary with the rate of fluid flow. This can be verified experimentally, as will be explained later.

β can be written as

$$\beta(f) = K_{eh} B + K_{gh} f \rho_g C_g \quad (4\text{-}8)$$

where K_{eh} = heat-absorption coefficient of environment in heating ($J/hr^{\circ}C\ m^2$); ($Btu/hr^{\circ}F.ft^2$)

K_{gh} = heat-absorption coefficient of fluidising gas in heating (l/kg); (l/lb)

f = flow (m^3/hr); (ft^3/hr)

ρ_g = density of fluidising gas (kg/m^3); (lb/ft^3)

C_g = heat capacity of fluidising gas ($J/^{\circ}C$); ($Btu/^{\circ}F$)

$K_{eh}B$ is the heat emitted to the environment, and $K_{gh}\,\rho_g\,C_g\,f$ is the heat emitted to the fluidising gas, which represents the flow-dependent component of the heat emission coefficient β. Experimental results (see Figs.A-5, A-6) show that there is a flow-dependent time delay in the system, which can be characterised as a linear function of flow

$$L(f) = m_L f + n_L \qquad (4\text{-}9)$$

Thus flow-dependent heating curve can be written as

$$\theta(t',f) - \theta(o) = \frac{Q}{\beta(f)}\left[1 - \exp\left(-\frac{\beta(f)}{\Sigma m_i C_i}\right) t'\right] \qquad (4\text{-}10)$$

where $\theta(o)$ = initial temperature of the l.p.i. in the bed

t' = delayed time, $(t - L)$

L = time delay of the system at the considered flow f

The heating time constant is

$$\tau_h = \frac{\Sigma m_i C_i}{\beta} \qquad (4\text{-}11)$$

and the maximum temperature, or system gain, is

$$\theta(\infty) - \theta(o) = \frac{Q}{\beta} \qquad (4\text{-}12)$$

On substitution of $\beta(f)$ from Eq. (4-8), the time constant τ_h and maximum temperature $\theta(\infty)$ can be evaluated

$$\tau_h(f) = \frac{\Sigma m_i C_i}{K_{eh} B + (K_{gh} \rho_g C_g) f} \qquad (4\text{-}13)$$

$$\theta(\infty,f) - \theta(o) = \frac{Q}{K_{eh} B + (K_{gh} \rho_g C_g) f} \qquad (4\text{-}14)$$

Eq. (4-10) together with Eq. (4-8) gives $\beta(f)$ in terms of flow f, and this represents the system for any flow and any time. The heating trajectory in the Laplace domain is

$$\theta(s,f) = \frac{\theta(o)}{s} + \frac{Q}{\beta(f)s} - \frac{\frac{Q}{\beta(f)} \exp\left[-sL(f)\right]}{1 + s\frac{\Sigma m_i C_i}{\beta(f)}} \qquad (4\text{-}15)$$

In the analysis of the heating and cooling of the system, it will be assumed that the effect of change of temperature on the gaseous and solid properties of the bed will be negligible. This is a reasonable assumption for a wide range of common industrial processes.

4.2.3. Experimental procedure

A typical heating response for $f = f_o$ is shown in Fig. 4-4. (The experimental curves are shown in Figs.A-6,A-7). The time constant and maximum temperature can be determined from this curve and

Eq. (4-14) can be constructed from this experimental data. Repeating the heating experiment for various flows reveals the time-constant/flow and temperature maxima/flow (or gain/flow) relationships that correspond to Eqs. (4-13) and (4-14). Due to the non-uniform and uncertain nature of the directly-heated bed, it is not easy to get clear temperature/time response curves. Similar observations have been reported regarding resistance measurements[16]. Consequently, an alternate method has been proposed which is based on Eq. (4-2) and which does not completely cater for the flow-dependence of the bed[16].

FIG. 4-4

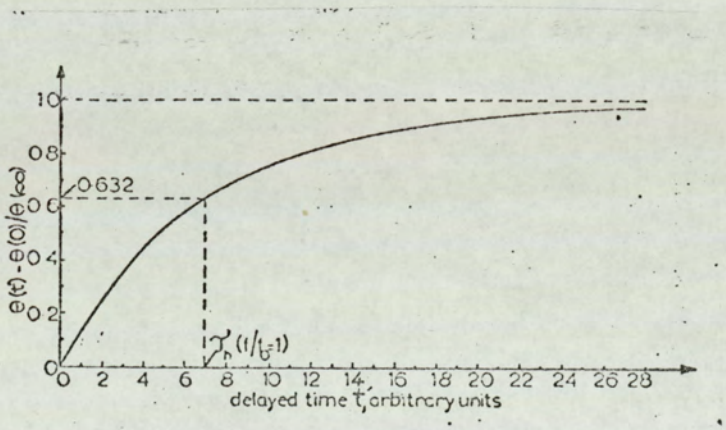

FIG. 4-4: Typical heating response of the system.

However, the simplified modified differential equation leads to the solution of Eq. (4-10) was used in this experimental procedure, and was found to be satisfactory for the study of practical processes. The heat energy per unit time Q is proportional to the electrical power input

$$Q = \mu P \qquad (4\text{-}16)$$

where μ is a constant dependent on the system of units used.

We can rewrite Eq. (4-14)

$$\theta(\infty,f) - \theta(o) = K_p(f)\, P \qquad (4\text{-}17)$$

where
$$K_p(f) = \frac{\mu}{K_{eh}B + (K_{gh}\,\rho_g C_g)\, f} \qquad (4\text{-}18)$$

For a given flow, temperature maxima are measured for varying electrical powers, corresponding to Eq. 4-17. If this experiment is repeated for different flow rates, a family of such straight lines is obtained. Such a family is displayed in Fig. 4-5, using normalised axes. The inverse slopes of this family of lines (Fig. 4-5) are displayed against normalised flow in Fig. 4-6; this slope/flow relationship can be expressed as

$$\frac{1}{K_p(f)} = \frac{K_{eh}B}{\mu} + \left[\frac{(K_{gh}\,\rho_g\, C_g)}{\mu}\right] f \qquad (4\text{-}19)$$

It can be observed from Fig. 4-5 that the family of temperature-maxima/power-input linear relationships fall into two groups above and below the condition corresponding to minimum fluidisation flow, i.e. the change from a fixed bed to a fluidised bed. This corresponds to the large change in slope, as the bed becomes fluidised, that is displayed in Fig. 4-6 by the dotted line.

The slope in Eq. (4-19) can be expressed as

$$M_p = \frac{K_{gh}\,\rho_g\, C_g}{\mu} \qquad (4\text{-}20)$$

FIG. 4-5

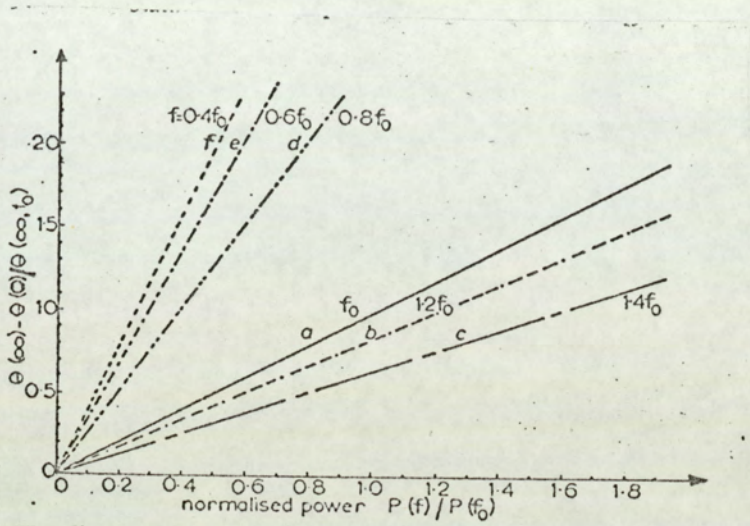

FIG. 4-5: Temperature-maxima (or system gain)/electrical-power input relationship,

a,b,c normal bed operation as a fluidised bed,

a) $K_p(f_o)_N = 1.0$

b) $K_p(1.2\ f_o)_N = 0.832$ (see Fig. 4-6)

c) $K_p(1.4\ f_o)_N = 0.66$

d,e,f bed operation without fluidisation,

d) $K_p(0.8\ f_o)_N = 2.63$

e) $K_p(0.6\ f_o)_N = 3.46$ (see Fig. 4-6)

f) $K_p(0.4\ f_o)_N = 5.0$

Eq. (4-20) will change according to the rate of flow, and particularly according to whether or not the bed is fluidised ($f > f_o$ or $f < f_o$). The salient factor in Eq. (4-20) which will change with the fluidising of the bed is the heat-absorption coefficient of the fluidising gas, K_{gh}. Thus, there are two significant values of K_{gh} which correspond to the unfluidised ($0 < f < f_o$) and the fluidised ($f_o < f < 1.4\ f_o$)

bed. Thus, for the class of beds studied, in which the normal operation is within the range $f_o < f < 1.4\ f_o$, there is a definite flow-independent value of M_p. Similarly, there is another definite value of M_p that corresponds to flow below the minimum for fluidisation. This is apparent from Fig. (4-6). Note also from Fig. (4-6) that the two lines, representing flow above and below the minimum for fluidisation intersect at a point on the ordinate corresponding to

$$\frac{K_{eh}\ B}{\mu} \qquad (4\text{-}21)$$

Expression (4-21) represents the heat emission to the environment and is, as is to be expected, flow-independent.

A practical procedure for determining the characteristics of new, or proposed, beds is as follows

a) M_p and $\frac{K_{eh}\ B}{\mu}$ can be evaluated from Fig. (4-6) and hence

$$\frac{\beta(f)}{\mu} = M_p(f) + \frac{K_{eh}\ B}{\mu} \qquad (4\text{-}22)$$

(Note that Eq. (4-22) corresponds to Eq. (4-8).)

Thus β can be evaluated for every rate of flow.

b) The temperature maximum can be found from Fig. (4-5), see Eq. (4-14) for the desired flow rate f and heat energy Q

$$\frac{Q}{\beta(f)} \qquad (4\text{-}23)$$

Thus, the temperature maxima are known for every flow rate (Fig. 4-8).

c) Using a typical heating curve, say Fig. 4-4, the time constant can be evaluated (see Eq. (4-11))

$$\tau_h = \frac{\Sigma m_i C_i}{\beta}$$

Since β is known, $\Sigma m_i C_i$ can be evaluated

$$\Sigma m_i C_i = \beta \tau_h \qquad (4\text{-}24)$$

$\Sigma m_i C_i$ remains unchanged, of course, for every time and rate of flow.

d) From the graph which corresponds to Eq. (4-9) we determine

$$L(f) = m_L f + n_L \qquad (4\text{-}25)$$

Then the $\theta(t',f)$ relationship can be constructed see Eq. (4-10). Using Eq. (4-22), the complete flow-dependent relationship can be obtained. Eqs. (4-22), (4-23) and (4-24) permit evaluation of the time constant $\tau_h(f)$ (see Eq. (4-13), and the temperature maxima (see 4-14).

Curve a in Fig.4.7 shows the variation of the time constant $\tau_h(f)$ with flow. This curve was constructed by measuring the heating-time constant for differing flow rates. Curve b in Fig.4.7 was derived by using the theoretical evaluation, (Eq.(4.13)) within the normal operating region ($f_, <f<1.4fo$). $\Sigma m_i C_i$ was determined experimentally for $f=fo$ in the manner described above (Eq.(4.24)). It can be seen from Fig.4.7 that within the normal-operation flow region the time-constant/flow relationship can be taken as linear.

Figure 4-8 display was compiled with the aid of Fig. 4-5. If any two of the following three quantities are known, the third can be determined from Fig. 4-5:

(i) Flow rate

(ii) Electrical power input

(iii) Temperature maxima (system gain).

Fig. 4-9 displays the normalised electrical-power input/flow relationship for constant maximum temperature. From Eqs. (4-14) and (4-16) the electrical-power input can be determined.

$$P(f) = \frac{\left[\theta(\infty,f)-\theta(o)\right]\left[K_{eh}B\right]}{\mu} + \frac{\left[\theta(\infty,f)-\theta(o)\right]\left[K_{gh}\rho_g C_g\right]}{\mu} f \Bigg|_{\theta(\infty,f) = \text{const.}} \qquad (4\text{-}26)$$

Eq. (4-26) can then be simplified:

$$P(f) = N_p + (M_p)\, f \qquad (4\text{-}27)$$

Eq. (4-27) corresponds with Fig. 4-9

By following the same analysis of Fig. 4-6, we expect, in Fig. 4-9, a smaller slope for $f < f_o$. The slope line for $f < f_o$ will intersect the ordinate at a value corresponding to the first term of Eq. (4-26), i.e. N_p in Eq. (4-27).

FIG. 4-6

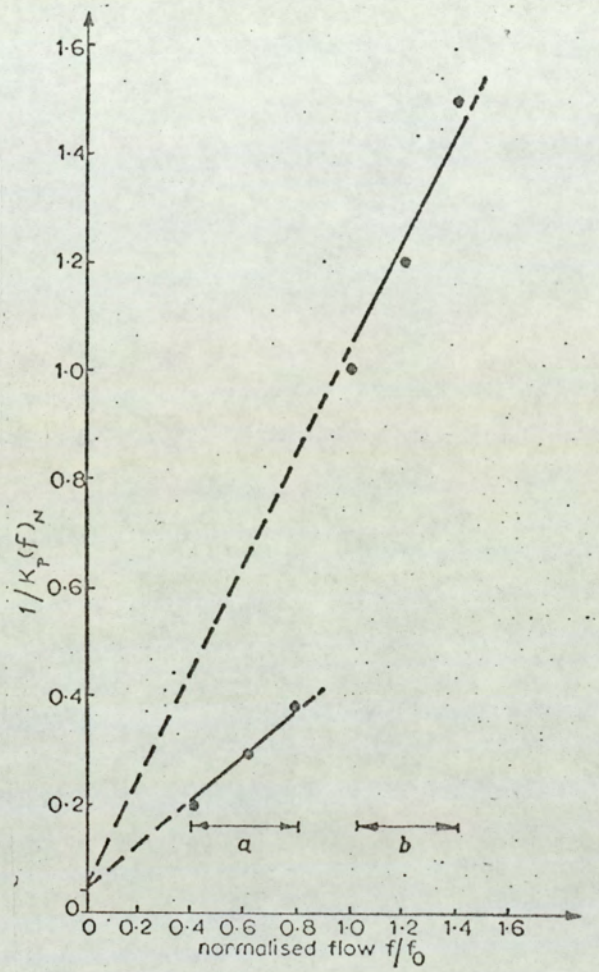

FIG. 4-6: Inverse-slope/flow relationship derived from Fig. 4- 5,

a) bed operation without fluidisation,

b) normal bed operation.

Curve a in Fig. 4-7 shows the variation of the time constant τ_h (f) with flow. This curve was constructed by measuring the heating-time constant for differing flow rates. Curve b in Fig. 4-7 was derived by using the theoretical evaluation, Eq. (4-13), within the normal operating region ($f_o \leq f \leq 1.4\ f_o$). $\Sigma m_i C_i$ was determined experimentally for $f = f_o$ in the manner described above Eq. (4-24). It can be seen from Fig. 4-7 that within the normal-operation flow region the time-constant/flow relationship can be taken as linear.

FIG. 4-7

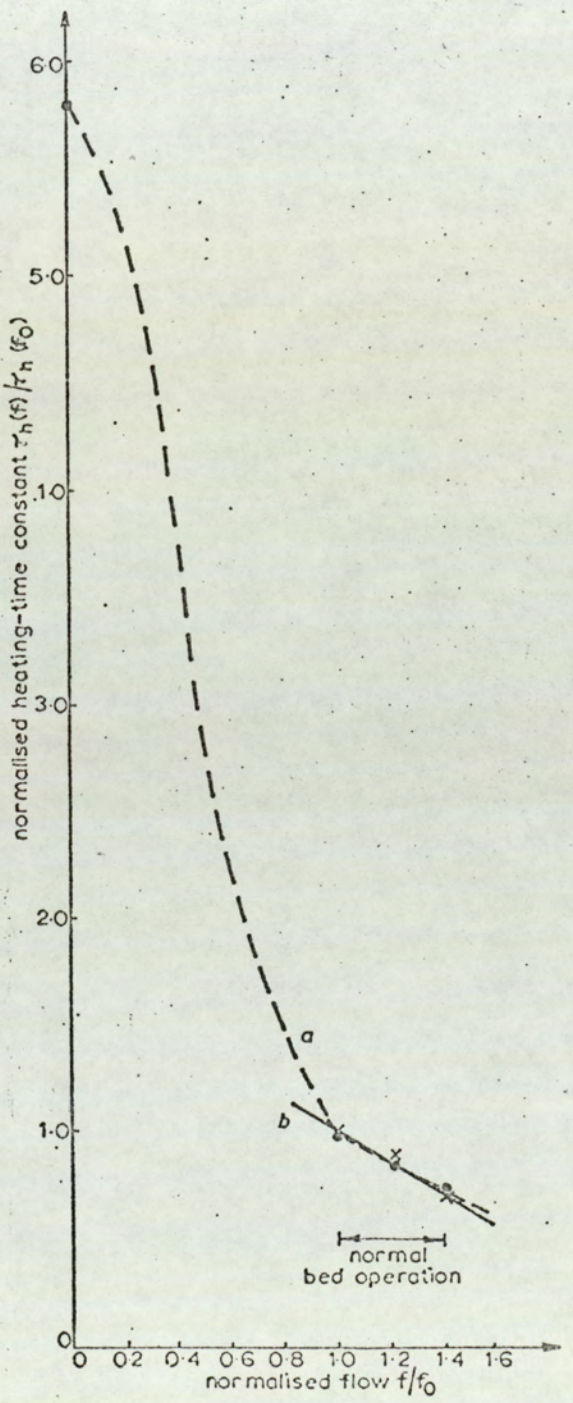

FIG. 4-7: Typical flow dependence of the heating time constant,

a) experimental curve

b) calculated curve

In Fig. 4-8 the normalised temperature-maxima/flow relationship is displayed for constant electrical-power input (see Eqs. (4-14), (4-23).

FIG. 4-8

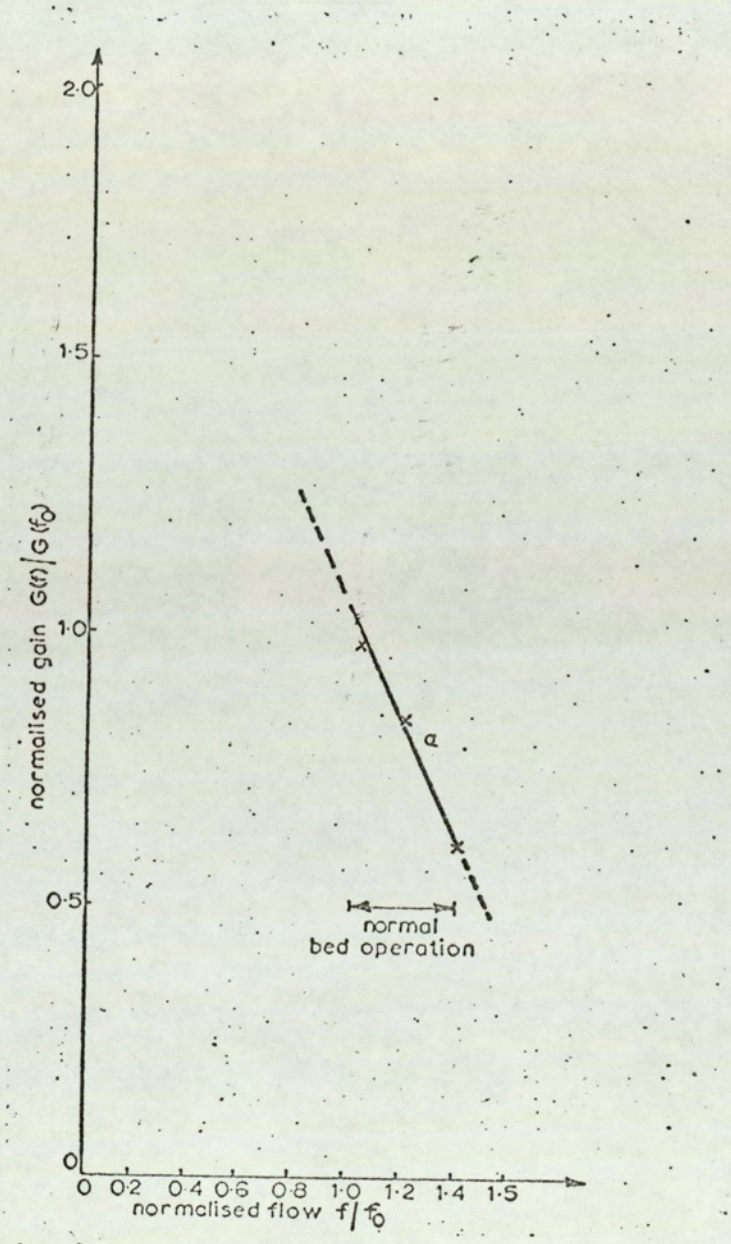

FIG. 4-8: Typical flow dependence of system gain for constant electric-power input.

$P(f) = \text{const.} = P(f_o)$

FIG. 4-9

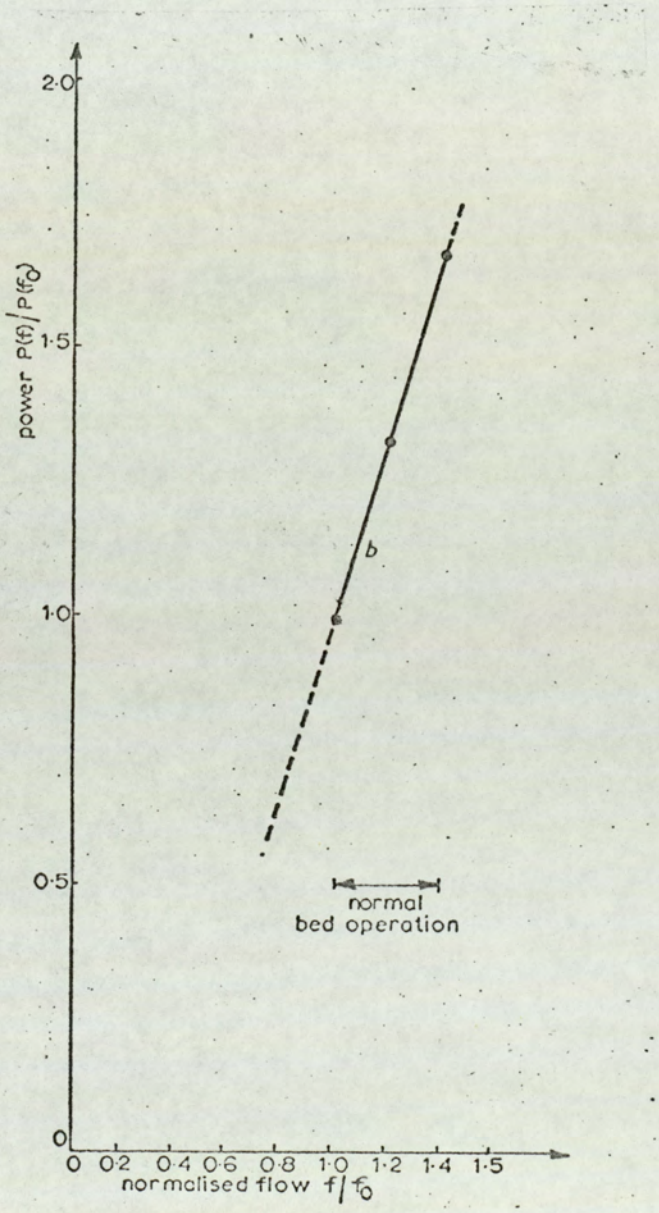

FIG. 4-9: Typical flow dependence of electrical-power input for constant system gain.

$$\theta(\infty,f) = \text{const.} = \theta(\infty,f_o)$$

4.3. Cooling

For the temperature-independent heat-emission case, the differential equation for cooling is

$$\Sigma m_i C_i \frac{d\left[\theta_c(t)\right]}{dt} + \gamma(f_c)\left[\theta_c(t) - \theta(o)\right] = 0 \qquad (4\text{-}28)$$

where γ = Temperature-independent coefficient of heat emission to the environment and to the fluidising gas during cooling ($J/hr^{\circ}C$); ($Btu/hr^{\circ}F$)

The solution to Eq. (4-28) is

$$\theta_c(t,f_c,f_h) = \theta(o) + \frac{Q}{\beta(f_h)}\left[\exp -\left(\frac{\gamma(f_c)}{\Sigma m_i c_i}\right) t\right] \qquad (4\text{-}29)$$

As in the heating case, Eq. (4-8), (f_c) can be written as

$$\gamma(f_c) = K_{ec} B + K_{gc} \rho_g C_g f_c \qquad (4\text{-}30)$$

where K_{ec} = heat absorption coefficient of environment in cooling ($J/hr^{\circ}C.m^2$); ($Btu/hr.^{\circ}F.ft^2$)

K_{gc} = heat absorption coefficient of fluidising gas in cooling (l/kg); (l/lb)

f_h = fluidising gas flow in heating (m^3/hr); (ft^3/hr)

f_c = fluidising gas flow in cooling (m^3/hr); (ft^3/hr)

FIG. 4-10

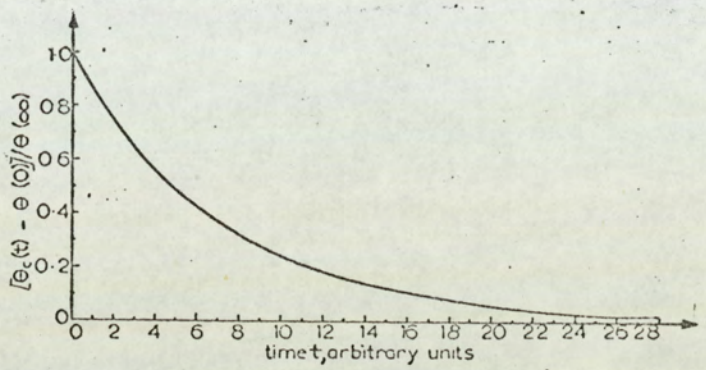

FIG. 4-10: Typical cooling response of the system (see also Figs.A-7,A-8)

A typical cooling curve for $f = f_o$ is shown in Fig. 4-10. No significant time delay was observed for the cooling mode. The time constant and maximum temperature $Q/\beta(f_h)$ (see Eq. (4-29) can be determined from Fig. 4-10. Repeating the cooling experiment for various flows, time-constant/flow relationship (see Eqs. (4-29) and (4-30), can be constructed (see Fig. 4-11).

$$\tau_c(f) = \frac{\Sigma m_i C_i}{\gamma(f_c)} = \frac{\Sigma m_i C_i}{K_{ec} B + K_{gc} \rho_g C_g f_c} \qquad (4\text{-}31)$$

$\Sigma m_i C_i$ in Eq. (4-31) is known from Eq. (4-24). As is seen from Fig. 4-11, in the normal operation region ($f_o \lesssim f \lesssim 1.4\ f_o$), the cooling-time-constant/flow relationship can be taken as linear. The temperature-maxima/flow relationship is known from Eq. (4-23). The cooling trajectory in the Laplace domain is

$$\theta(s,f_h,f_c) = \frac{\theta(o)}{s} + \frac{\dfrac{Q}{\beta(f_h)}}{1 + s\dfrac{\Sigma m_i C_i}{\gamma(f_c)}} \qquad (4\text{-}32)$$

FIG. 4-11

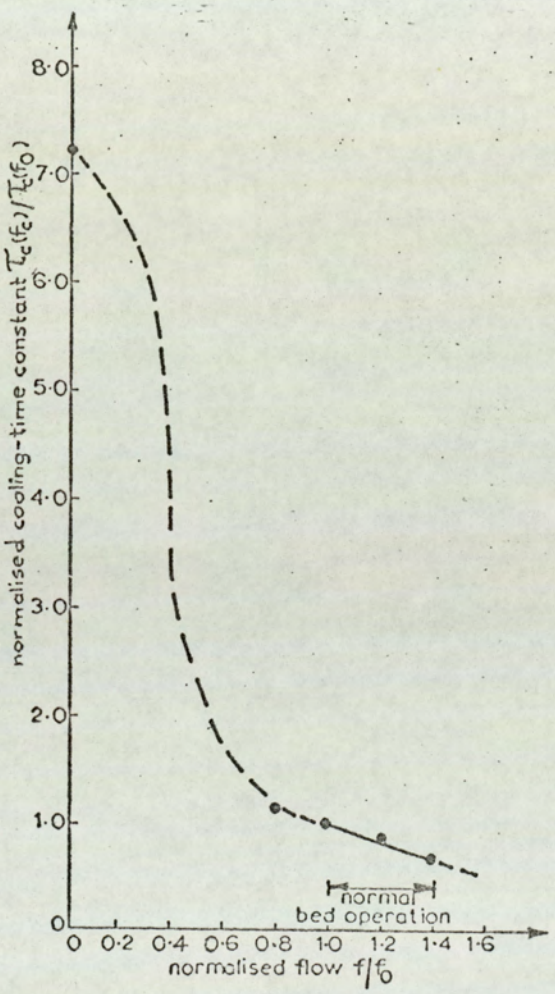

FIG. 4-11: Typical flow dependence of cooling time constant.

4.4. Resistivity

Although there is no generally recognised theoretical analysis for the resistance of a conducting fluidised bed, some useful information is contained in the literature. The electrical resistance of a fluidised

bed has been studied experimentally, and suggestions have been made as to the conduction mechanism [17,10]. The effects of various geometrical and other factors on the electrical properties of certain beds[18], and arcing phenomena within beds has been studied[15]. Information on the conductivity mechanism, the resistances of certain materials, resistance/temperature relationships and design considerations has been published[16,19,20].

Direct measurement of the resistance in a fluidised bed is difficult because of the nonuniform and uncertain nature of the bed. A large number of experiments must be conducted to determine a meaningful average value. To overcome such difficulties, an indirect method has been suggested[16]. This is based on measuring the maximum temperature within the bed. A modification of the method used above to study the heating mode of a bed can be adapted to determine satisfactorily the bed resistance.

Consider the electrical-power input

$$P = VI = \frac{V^2}{R} \qquad (4\text{-}33)$$

where V = applied voltage across the electrodes (volt)

I = current through the bed (ampere)

R = bed resistance between the electrodes (ohm)

Although the total resistance consists of the contact resistance between electrodes and particles, the contact resistance between particles and the resistance of the particles, the bed resistance can be considered as the resistance seen between the electrodes.

$$R = \frac{V^2}{P} \qquad (4\text{-}34)$$

Using Eqs. (4-17) and (4-18) we can write the electrical-power input equation

$$P = \frac{\left[\theta(\infty,f) - \theta(o)\right]\left[K_{eh}B + K_g \rho_g C_g) f\right]}{\mu} \qquad (4\text{-}35)$$

then:

$$R = \frac{V^2 \mu}{\left[\theta(\infty,f) - \theta(o)\right]\left[K_{eh}B + (K_{gh} \rho_g C_g) f\right]} \qquad (4\text{-}36)$$

In curve a of Fig. 4-12 the resistance characteristic corresponding to Eq. (4-36) is displayed. This is obtained by measuring the maximum temperature in the bed and determining the corresponding electrical-power input P by use of the curve of Fig. 4-5, which corresponds to the operation flow. Thus, using Eq. (4-34), R is found and curve a of Fig. 4-12 can be constructed.

The average resistance of different flows is found by direct measurement. Curve b of Fig. 4-12 is the experimental curve so obtained. It compares favourably with the semi experimental results (curve a of Fig. 4-12).

4.5. Conclusions

(a) For a class of directly electrically heated fluidised beds, of circular cross section, with fixed-bed-height/radius ratios in the region of unity, with materials similar to 60-mesh coke, a practical, simplified, modified heating model and a new cooling model, have been developed.

FIG. 4-12

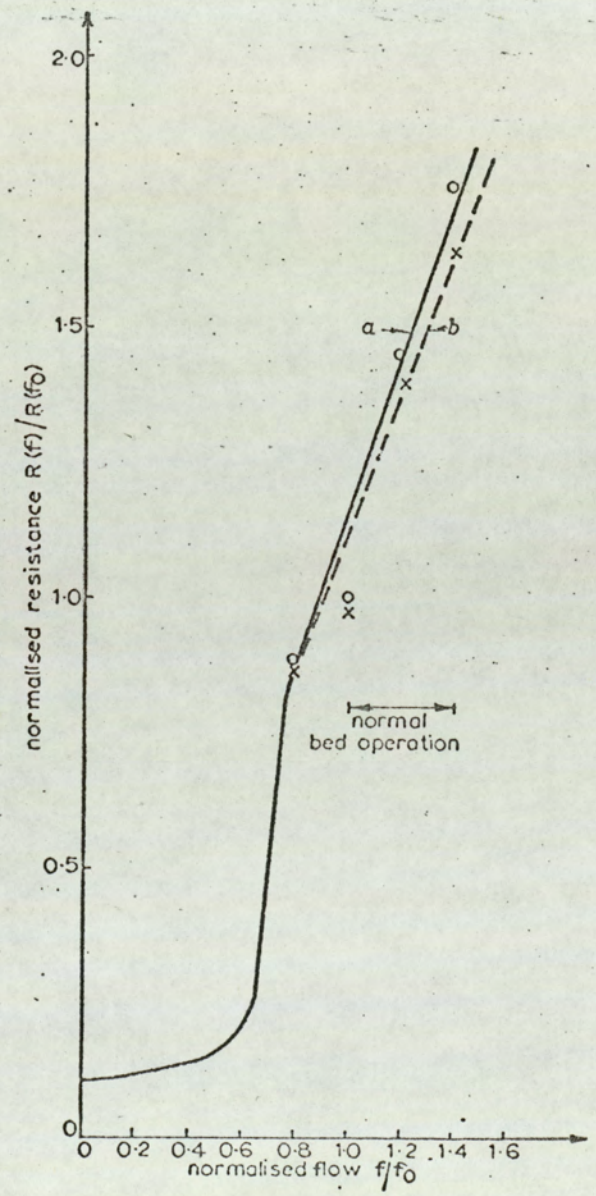

FIG. 4-12: Typical flow dependence of the bed resistance,

a) calculated curve

b) experimental curve

(b) These models can be derived experimentally by simple tests at different flow rates, e.g. at three flow rates in the range $f_o < f < \alpha f_o$ where α is a constant greater than one (usually 1.4 in the class of beds studied).

(c) The curves constructed from these tests provide a facile method for determining the important bed parameters: flow, electrical-power input and maximum temperature. If any two of these are known, the third can be evaluated from the curves (see Fig. 4-5).

(d) A modified practical indirect method has been developed for determining the average bed resistance. This overcomes the measurement difficulties associated with direct methods.

(e) These models are intended to be helpful in designing and operating existing, and proposed temperature-control systems for the fluidised beds. The theoretical and experimental methods used may also be helpful in deriving models for other control systems, e.g. control by changing the effective electrode area dipped into the bed[14].

5
FLOW DIAGRAM MODELS OF THERMAL PROCESSES

5.1. Introduction.

In the study of a process, simple diagrams which can represent the process are quite essential to facilitate analysis and design. In complex processes involving many stages, even block diagrams are too complicated to follow the actual phenomena in the process.

In this study, new flow diagrams are presented that represent a class of heat-transfer processes and which enable the determination of final temperatures in a simple straightforward procedure.

Although fluidised beds are studied as an interesting example, the method is equally applicable to many other processes which involve this kind of heat-balance equation.

In the diagrams all final temperature levels and materials involved are represented by geometric figures and branches between them. The rules about the construction and use of flow diagrams are derived and presented in logical steps after finding their relations to the actual process equations.

5.2. Flow diagram representation

As an illustrative example, consider a fluidised bed process in which the solid particles and fluid, gas or liquid, temperatures are raised from θ_0 to θ_R. The schematic diagram of such a system is shown in Fig. 5-1

FIG. 5-1

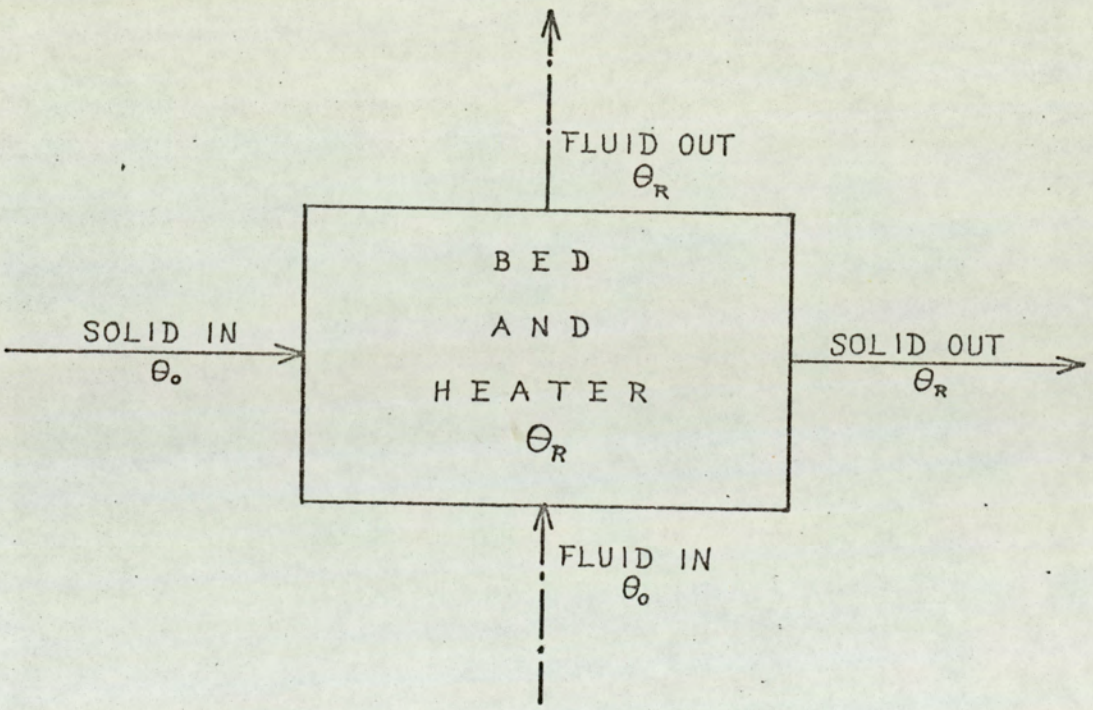

FIG. 5-1: Schematic diagram of a fluidised bed.

Thermal input to raise bed temperature to θ_R from θ_0 is

$$Q_{(\theta_R,\theta_0,0)} = W_f C_f(\theta_R - \theta_0) + W_s C_s(\theta_R - \theta_0) \qquad (5\text{-}1)$$

where $Q_{(\theta_R, \theta_O, O)}$ = thermal input to raise bed temperature to θ_R, from θ_O, with zero heat exchangers (J/hr); (Btu/hr)

W_f = flow rate of fluid (kg/hr); (lb/hr)

W_s = flow rate of particulate solid (kg/hr); (lb/hr)

C_f = specific heat of fluid (J/kg.deg); (Btu/lb°F)

C_s = specific heat of particulate solid. (J/kg.deg) (Btu/lb°F)

θ_O = initial temperature (°C); (°F)

θ_R = final temperature (°C); (°F)

Such a process can be shown as a flow diagram as displayed in Fig. 5-2. Squares and triangles are used in Fig. 5-2 to clearly show the different temperature states.

FIG 5-2

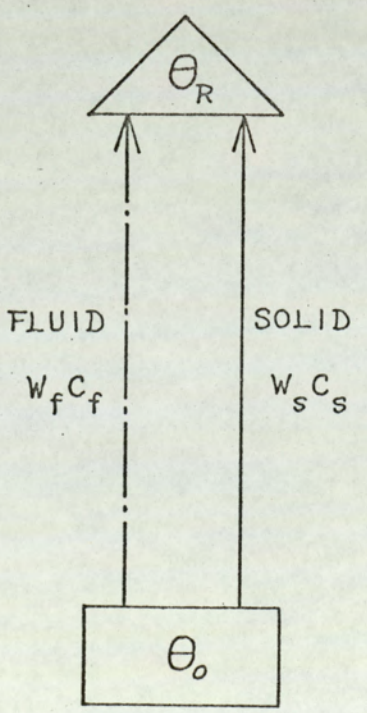

FIG. 5-2: Flow diagram of the fluidised bed process in Fig. 5-1.

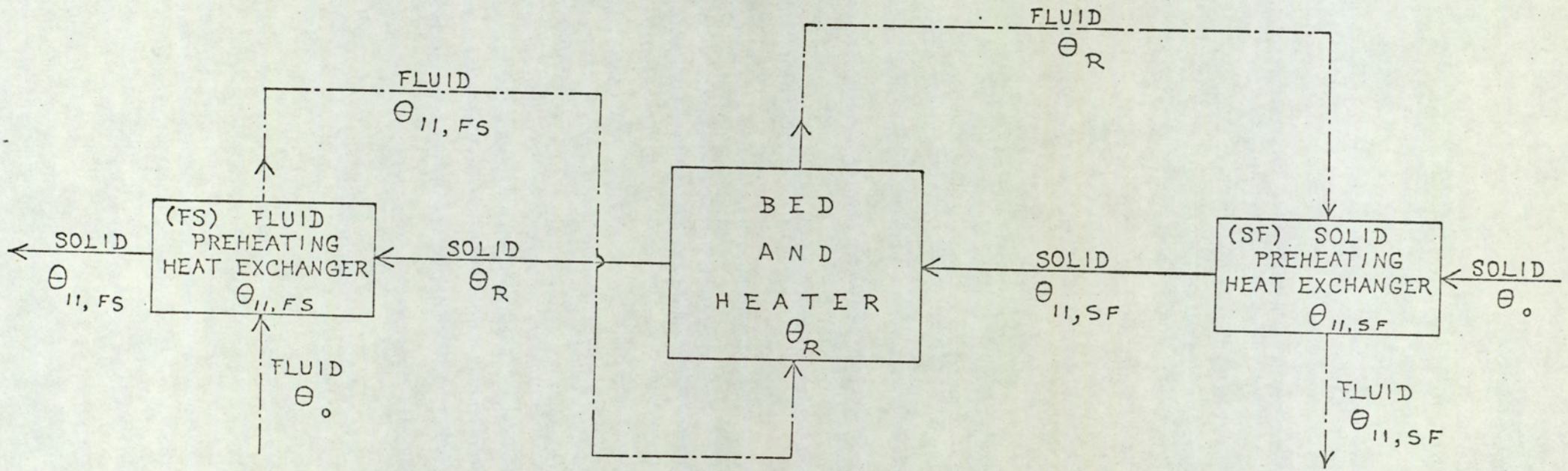

FIG. 5.3: Schematic diagram of a fluidised bed with one stage (FS) for preheating the fluid and one stage (SF) for preheating the solid.

Now consider another process, in which the outgoing solid preheats the incoming fluid and the outgoing fluid preheats the incoming solid. Such a process is shown schematically in Fig. 5-3 and as a flow diagram in Fig. 5-4.

A comparison of Figs. 5-3 and 5-4 shows the clarity of the flow diagram when compared with the schematic diagram. In this process the thermal input is

$$Q_{(\theta_R,\theta_O,1F,1S)} = W_f C_f(\theta_R - \theta_{11,FS}) + W_s C_s(\theta_R - \theta_{11,SF}) \quad (5\text{-}2)$$

where $Q_{(\theta_R,\theta_O,1F,1S)}$ = thermal input to raise the bed temperature to θ_R from θ_O with 1 stage of preheating the fluid by the heated solid and 1 stage of preheating the solid by the heated fluid.

$\theta_{11,FS}$ = final temperature state of a particular heat exchanger. The first subscript (1) identifies the individual heat exchanger under consideration. The second subscript (1) identifies the total number of heat exchangers of type FS in the system. The subscript F identifies the preheated materials as fluid. The subscript S identifies the preheating agent as solid. Thus the final temperature state of heat exchanger 'i', of an 'n' heat exchanger system, in which a solid is preheated by a fluid is identified as $\theta_{in,SF}$.

$\theta_{11,SF}$ = Final temperature state of the heat exchanger in which a solid is preheated by a fluid.

FIG. 5-4

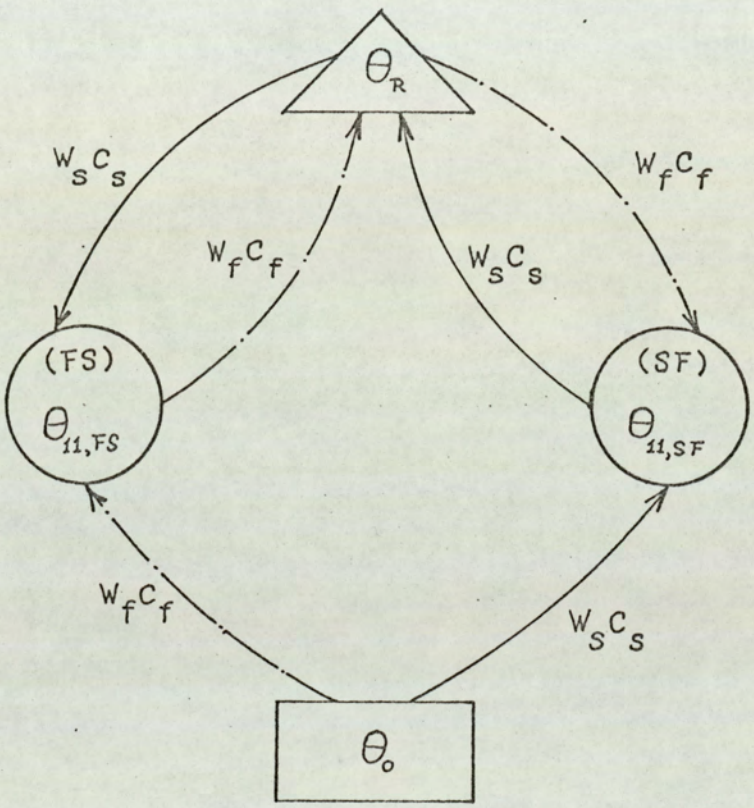

FIG. 5-4: Flow diagram of a fluidised bed with one stage (FS) for preheating the fluid, and one stage (SF) for preheating the solid.

$Q_{(\theta_R,\theta_O,1F)}$ can be derived in another way. The thermal input should be equal to the total heat absorbed by the solid and fluid, to raise their temperature, less the heat contributed by the solid and fluid, in their preheating function.

$$Q_{(\theta_R,\theta_O,1F,1S)} = W_f C_f(\theta_{11,FS} - \theta_O) + W_f C_f(\theta_R - \theta_{11,FS}) + W_s C_s(\theta_{11,SF} - \theta_O) + W_s C_s(\theta_R - \theta_{11,SF}) - W_s C_s(\theta_R - \theta_{11,FS}) - W_f C_f(\theta_R - \theta_{11,SF}) \quad (5\text{-}3)$$

Consider the heat balance for the heat exchanger (FS)

$$W_s C_s(\theta_R - \theta_{11,FS}) = W_f C_f(\theta_{11,FS} - \theta_O) \quad (5\text{-}4)$$

and that for the heat exchanger (SF)

$$W_f C_f(\theta_R - \theta_{11,SF}) = W_s C_s(\theta_{11,SF} - \theta_O) \quad (5\text{-}5)$$

Considering Eqs. (5-3), (5-4), and (5-5), we can write

$$Q_{(\theta_R,\theta_O,1F,1S)} = W_f C_f(\theta_R - \theta_{11,FS}) + W_s C_s(\theta_R - \theta_{11,SF}) \quad (5\text{-}6)$$

From Eq. 5-3 we can also write

$$Q_{(\theta_R,\theta_O,1F)} = W_f C_f(\theta_R - \theta_O) + W_s C_s(\theta_R - \theta_O) - W_s C_s(\theta_R - \theta_{11,FS}) - W_f C_f(\theta_R - \theta_{11,SF}) \quad (5\text{-}7)$$

Considering Eq. (5-1)

$$Q_{(\theta_R,\theta_O,1F)} = Q_{(\theta_R,\theta_O,O)} - W_s C_s(\theta_R - \theta_{11,FS}) - W_f C_f(\theta_R - \theta_{11,SF}) \quad (5\text{-}8)$$

The reduction in the thermal input achieved will be identified as

$$Q_{(E,1F,1S)}$$

where 1st subscript (E) indicates an economy, saving, of thermal input.

2nd subscript (1F) indicates one stage to preheat fluid.

3rd subscript (1S) indicates one stage to preheat solid.

From Eq. (5-8)

$$\begin{aligned} Q_{(E,1F,1S)} &= Q_{(\theta_R,\theta_O,O)} - Q_{(\theta_R,\theta_O,1F)} \\ &= W_s C_s(\theta_R - \theta_{11,FS}) + W_f C_f(\theta_R - \theta_{11,SF}) \end{aligned} \qquad (5\text{-}9)$$

From Eq. (5-9) we notice that this reduction of thermal input corresponds to the downward arrows of Fig. 5-4.

From Eq. (5-6) we notice that the thermal input to be given to achieve the desired process temperature corresponds to the upward arrows between the final temperature and the preheating stage temperatures in Fig. 5-4.

Now consider a fluidised bed process with n stages to preheat the fluid with the heated solid and n stages to preheat the solid with the heated fluid. Flow diagram of this process is shown in Fig. 5-5.

Using similar arguments which were used to derive Eq. (5-3), we can find that in this process the thermal input is

$$
\begin{aligned}
Q_{(\theta_R,\theta_O,nF,nS)} = {} & W_f C_f(\theta_{nn,FS} - \theta_O) + W_f C_f(\theta_{(n-1)n,FS} - \theta_{nn,FS}) + \cdots \\
\cdots + {} & W_f C_f(\theta_{2n,FS} - \theta_{3n,FS}) + W_f C_f(\theta_{1n,FS} - \theta_{2n,FS}) \\
& + W_f C_f(\theta_R - \theta_{1n,FS}) \\
& - W_s C_s(\theta_{(n-1)n,FS} - \theta_{nn,FS}) - W_s C_s(\theta_{(n-2)n,FS} \\
& \qquad - \theta_{(n-1)n,FS}) - \cdots \\
\cdots - {} & W_s C_s(\theta_{1n,FS} - \theta_{2n,FS}) - W_s C_s(\theta_R - \theta_{1n,FS}) \\
& + W_s C_s(\theta_{nn,SF} - \theta_O) + W_s C_s(\theta_{(n-1)n,SF} - \theta_{nn,SF}) + \cdots \\
\cdots + {} & W_s C_s(\theta_{2n,SF} - \theta_{3n,SF}) + W_s C_s(\theta_{1n,SF} - \theta_{2n,SF}) \\
& + W_s C_s(\theta_R - \theta_{1n,SF}) \\
& - W_f C_f(\theta_{(n-1)n,SF} - \theta_{nn,SF}) - W_f C_f(\theta_{(n-2)n,SF} \\
& \qquad - \theta_{(n-1)n,SF}) - \cdots \\
\cdots - {} & W_f C_f(\theta_{1n,SF} - \theta_{2n,SF}) - W_f C_f(\theta_R - \theta_{1n,SF})
\end{aligned}
\qquad (5\text{-}10)
$$

Considering the heat balances for the preheating heat exchangers (circles in Fig. 5-5),and simplifying Eq. (5-10) accordingly we can write

$$
Q_{(\theta_R,\theta_O,nF,nS)} = W_f C_f(\theta_R - \theta_{1n,FS}) + W_s C_s(\theta_R - \theta_{1n,SF}) \qquad (5\text{-}11)
$$

From Eq. (5-11) we notice that the thermal input to be given to achieve the desired process temperature corresponds to the upward arrows between the final temperature and the first preheating-stage temperature. From Eq.(5-10) we also can write

$$Q_{(\theta_R,\theta_O,nF,nS)} = W_f C_f(\theta_R - \theta_O) + W_s C_s(\theta_R - \theta_O) - W_s C_s(\theta_R - \theta_{nn,FS}) - W_f C_f(\theta_R - \theta_{nn,SF}) \quad (5\text{-}12)$$

Using Eq. (5-1) we can write Eq. (5-12) as

$$Q_{(\theta_R,\theta_O,nF,nS)} = Q_{(\theta_R,\theta_O,O)} - W_s C_s(\theta_R - \theta_{nn,FS}) - W_f C_f(\theta_R - \theta_{nn,SF}) \quad (5\text{-}13)$$

The reduction in thermal input will be

$$Q_{(E,nF,nS)} = Q_{(\theta_R,\theta_O,O)} - Q_{(\theta_R,\theta_O,nF,nS)} = W_s C_s(\theta_R - \theta_{nn,FS}) + W_f C_f(\theta_R - \theta_{nn,SF}) \quad (5\text{-}14)$$

From Eq. (5-14) we notice that the reduction in thermal input corresponds to the downward arrows of Fig. 5-5.

The above method illustrates the ease with which heat balance equations and the reductions in the required thermal input are derived by the use of flow diagrams. Once the flow diagram is obtained for any thermal process, the heat balance equation can be written down by following a few simple rules outlined in a later section.

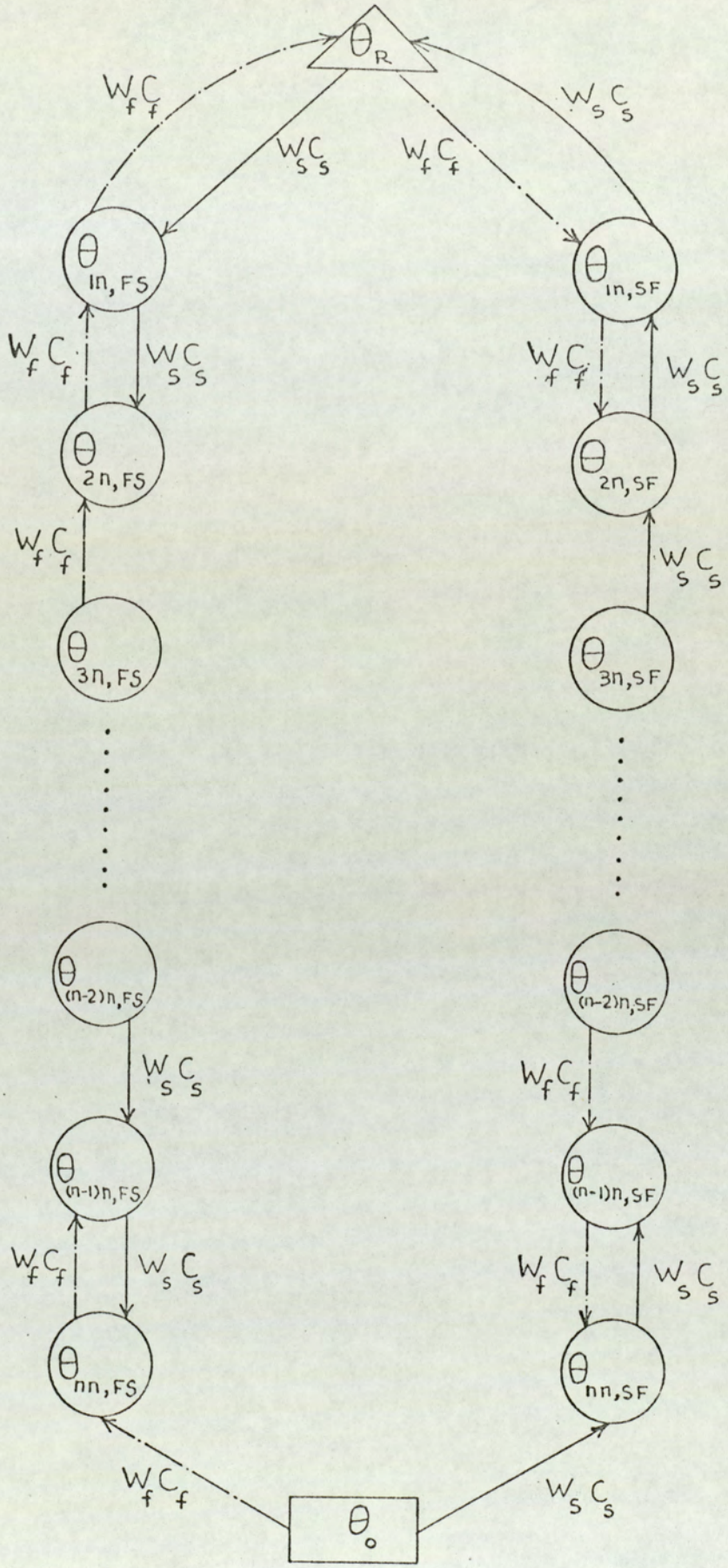

FIG. 5-5: Flow diagram of a fluidised bed process with "n" stages for preheating thefluid and "n" stages for preheating the solid.

5.3. Using the flow diagrams for a comparison between the two heat exchange processes.

As an example, consider a fluidised bed process (a) with one preheating stage for preheating the fluid and another process (b) with one preheating stage for preheating the solid. (Figs. 5-6 (a) and (b) respectively.

FIG. 5-6

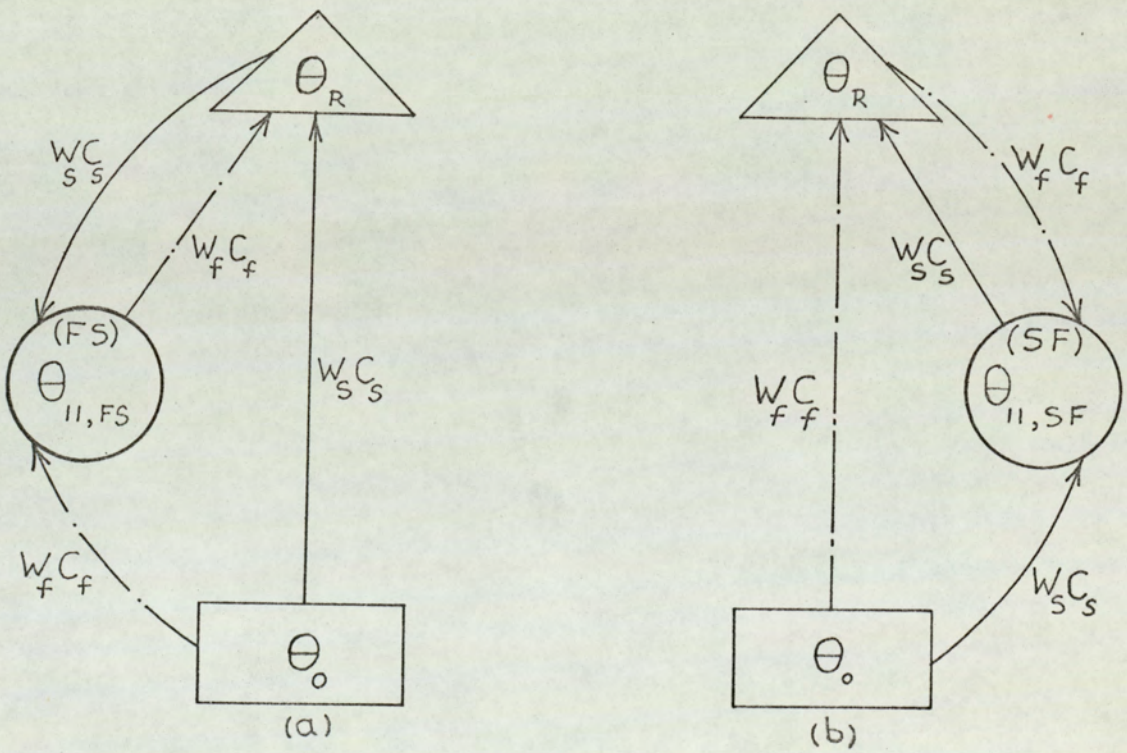

FIG. 5-6: Flow diagram of a fluidised bed with

a) one stage (FS) for preheating the fluid

b) one stage (SF) for preheating the solid.

In processes of this kind, it is often required that the thermal inputs for the two cases (a) and (b) to raise the process temperature to θ_R, be equal. It is proposed to derive this condition, using the flow diagrams.

Using the argument similar to the one used for deriving Eq. (5-3), we can write the thermal inputs as

Case (a)

$$Q_{(\theta_R,\theta_O,1F)} = W_s C_s(\theta_R - \theta_O) + W_f C_f(\theta_{11,FS} - \theta_O) + W_f C_f(\theta_R - \theta_{11,FS}) - W_s C_s(\theta_R - \theta_{11,FS}) \quad (5\text{-}15)$$

Case (b)

$$Q_{(\theta_R,\theta_O,1S)} = W_f C_f(\theta_R - \theta_O) + W_s C_s(\theta_{11,SF} - \theta_O) + W_s C_s(\theta_R - \theta_{11,SF}) - W_f C_f(\theta_R - \theta_{11,SF}) \quad (5\text{-}16)$$

To find the condition under which the thermal inputs for cases (a) and (b) be equal, we equate Eqs.(5-15) and (5-16). This simplifies to

$$W_s C_s(\theta_R - \theta_{11,FS}) = W_f C_f(\theta_R - \theta_{11,SF}) \quad (5\text{-}17)$$

The two sides of Eq. (5-17), however, also represent the terms corresponding to the downward arrows of Figs. 5-6 (a) and (b). It is, therefore, seen that condition Eq. (5-17) can be derived directly from this flow diagram without the use of the elaborate thermal balance equations. The flow diagrams also show the intermediate temperatures, and depict the process in a very clear manner, as opposed to the conventional block diagrams.

5.4. The processes which involve more than two materials.

In a process which involves three materials, (s), (f) and (y), we consider the cases: a) (s) preheats (f), (Fig. 5-7 (a)) and b) (f) preheats (y), (Fig. 5-7 (b)). We want to find the conditions under which the thermal inputs of the two processes are equal.

FIG. 5-7

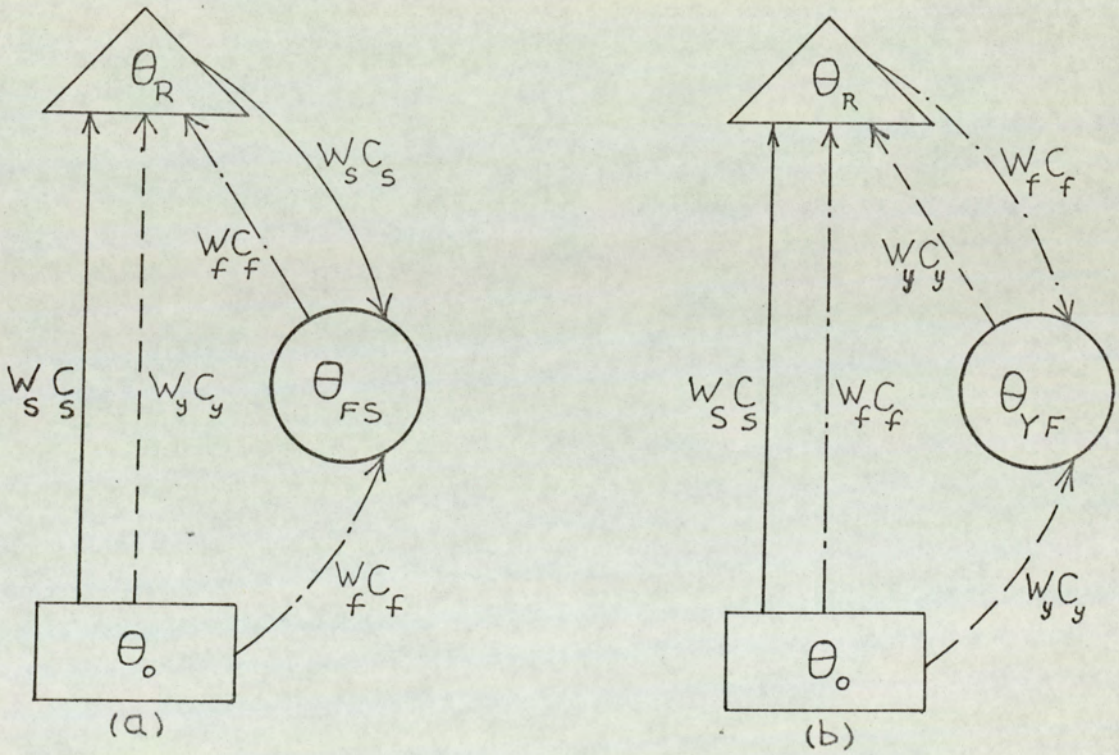

FIG. 5-7: Flow diagrams of three material processes.

(a) Material (s) preheats material (f)

(b) Material (f) preheats material (y)

Now we take a more general case in which the heat balance equation for the preheating heat exchanger is not used. In this case, there is not a simple heat exchange between the two materials in the preheating heat exchanger. Under this condition, the thermal input for case (a) is

$$Q_{(\theta_R,\theta_O,FS)} = W_sC_s(\theta_R - \theta_O) + W_yC_y(\theta_R - \theta_O) + W_fC_f(\theta_{FS} - \theta_O) + W_fC_f(\theta_R - \theta_{FS}) - W_sC_s(\theta_R - \theta_{FS}) \quad (5\text{-}18)$$

and for case (b)

$$Q_{(\theta_R,\theta_O,YF)} = W_sC_s(\theta_R - \theta_O) + W_fC_f(\theta_R - \theta_O) + W_yC_y(\theta_{YF} - \theta_O) + W_yC_y(\theta_R - \theta_{YF}) - W_fC_f(\theta_R - \theta_{YF}) \quad (5\text{-}19)$$

Eqs. (5-20) and (5-21) are the simplified forms of Eqs. (5-18) and (5-19) respectively.

$$Q_{(\theta_R,\theta_O,FS)} = W_sC_s(\theta_R - \theta_O) + W_yC_y(\theta_R - \theta_O) + W_fC_f(\theta_R - \theta_O) - W_sC_s(\theta_R - \theta_{FS}) \quad (5\text{-}20)$$

$$Q_{(\theta_R,\theta_O,YF)} = W_sC_s(\theta_R - \theta_O) + W_fC_f(\theta_R - \theta_O) + W_yC_y(\theta_R - \theta_O) - W_fC_f(\theta_R - \theta_{YF}) \quad (5\text{-}21)$$

Corresponding simplifications can also be done on the flow diagrams, as is shown in Figs. 5-8 (a) and (b) correspondingly.

FIG. 5-8

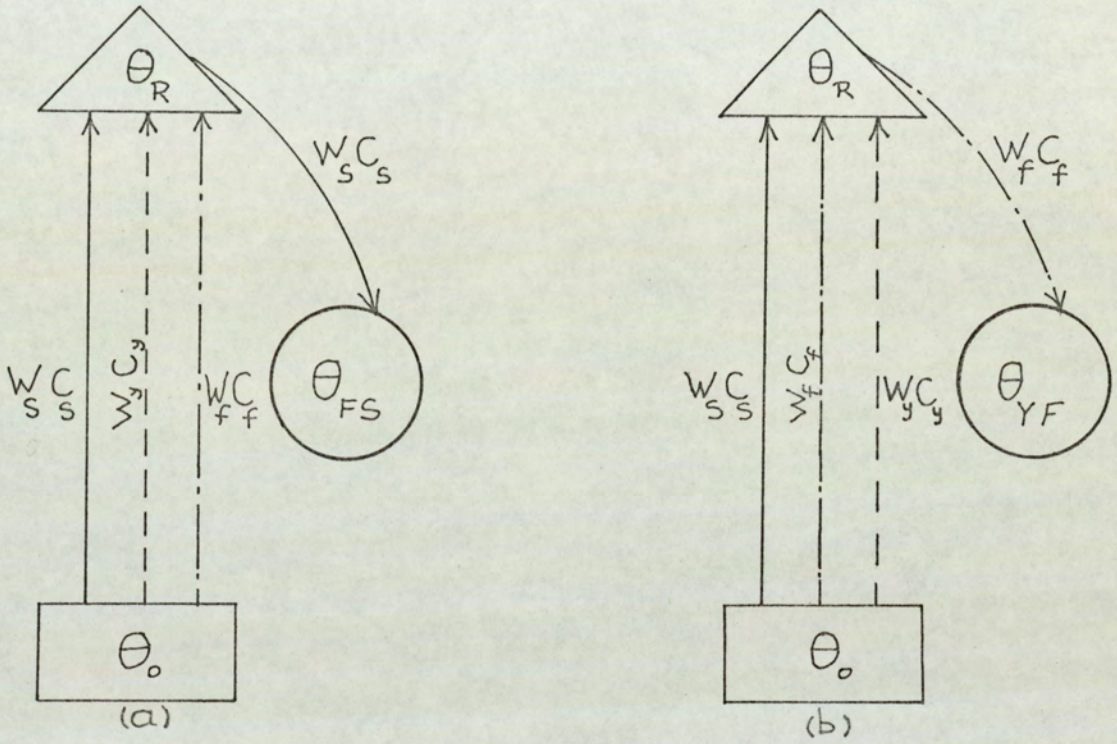

FIG. 5-8: Simplified flow diagrams of a three material process.

(a) Material (s) preheats material (f)

(b) Material (f) preheats material (y)

If we equate right hand sides of Eqs. (5-20) and (5-21), we obtain the condition

$$W_s C_s(\theta_R - \theta_{FS}) = W_f C_f(\theta_R - \theta_{YF}) \qquad (5\text{-}22)$$

This condition can directly be written from the diagrams Figs. 5-8 (a) and (b) by just equating the terms which correspond to the branches that are not the same in both diagrams, i.e. all the branches except the

one between θ_R and θ_{FS} in Fig. 5-8 (a) and between θ_R and θ_{YF} in Fig. 5-8 (b). In Eq. (5-22) the left-hand side corresponds to (θ_R, θ_{FS}) branch in Fig. 5-8 (a) and the right-hand side to (θ_R, θ_{YF}) branch in Fig. 5-8 (b). If we consider the heat balance equations for the preheating heat exchangers,then Eqs. (5-18) and (5-19) can be simplified to Eqs. (5-23) and (5-24) respectively.

$$Q_{(\theta_R,\theta_O,FS)} = W_s C_s(\theta_R - \theta_O) + W_y C_y(\theta_R - \theta_O) + W_f C_f(\theta_R - \theta_{FS}) \quad (5\text{-}23)$$

$$Q_{(\theta_R,\theta_O,YF)} = W_s C_s(\theta_R - \theta_O) + W_f C_f(\theta_R - \theta_O) + W_y C_y(\theta_R - \theta_{YF}) \quad (5\text{-}24)$$

Corresponding simplifications can also be done on the flow diagrams by cancelling the appropriate branches.

If we equate Eqs. (5-23) and (5-24),we obtain the condition

$$W_y C_y(\theta_R - \theta_O) + W_f C_f(\theta_R - \theta_{FS}) = W_f C_f(\theta_R - \theta_O) + W_y C_y(\theta_R - \theta_{YF}) \quad (5\text{-}25)$$

Eq. (5-25) can also be written directly from the simplified diagrams, using the similar argument used for writing Eq. (5-22) from Figs. 5-8 (a) and (b) directly.

The above analysis clearly brings out the advantages of the flow diagrams for complex heat transfer processes that involve more than two materials. The method also illustrates the simplification of flow diagrams once the overall diagram is derived, and this enables the evaluation of steady states in an easier way.

5.5 The processes which involve losses.

As an example, again consider a fluidised bed process with n stages to preheat the fluid with the heated solid and n stages to preheat the solid with the heated fluid, which is shown in Fig. 5-5. Now we consider the losses which may occur at each stage of the process. In this case, the argument which was used to derive Eq. (5-3) must be changed such that it should state that the thermal input should be equal to the total heat absorbed by the solid and fluid to raise their temperature, plus the losses, less the heat contributed by the solid and fluid in their preheating function. Also, in heat-balance equations, the heat contributed by the heating agent is equal to the heat absorbed by the preheated substance plus the heat loss at that stage.

The losses are shown as $\varepsilon_{in,FS}$ or $\varepsilon_{in,SF}$ and the subscripts are explained in connection with Eq. (5-2). The process shown in Fig. 5-5 can be re-drawn to include the losses as shown in Fig. 5-9. As an example, we write the heat balance equation for the second heat exchanger for preheated fluid case as

$$W_s C_s(\theta_{1n,FS} - \theta_{2n,FS}) = W_f C_f(\theta_{2n,FS} - \theta_{3n,FS}) + \varepsilon_{2n,FS} \qquad (5\text{-}26)$$

or for preheated solid case as

$$W_f C_f(\theta_{1n,SF} - \theta_{2n,SF}) = W_s C_s(\theta_{2n,SF} - \theta_{3n,SF}) + \varepsilon_{2n,SF} \qquad (5\text{-}27)$$

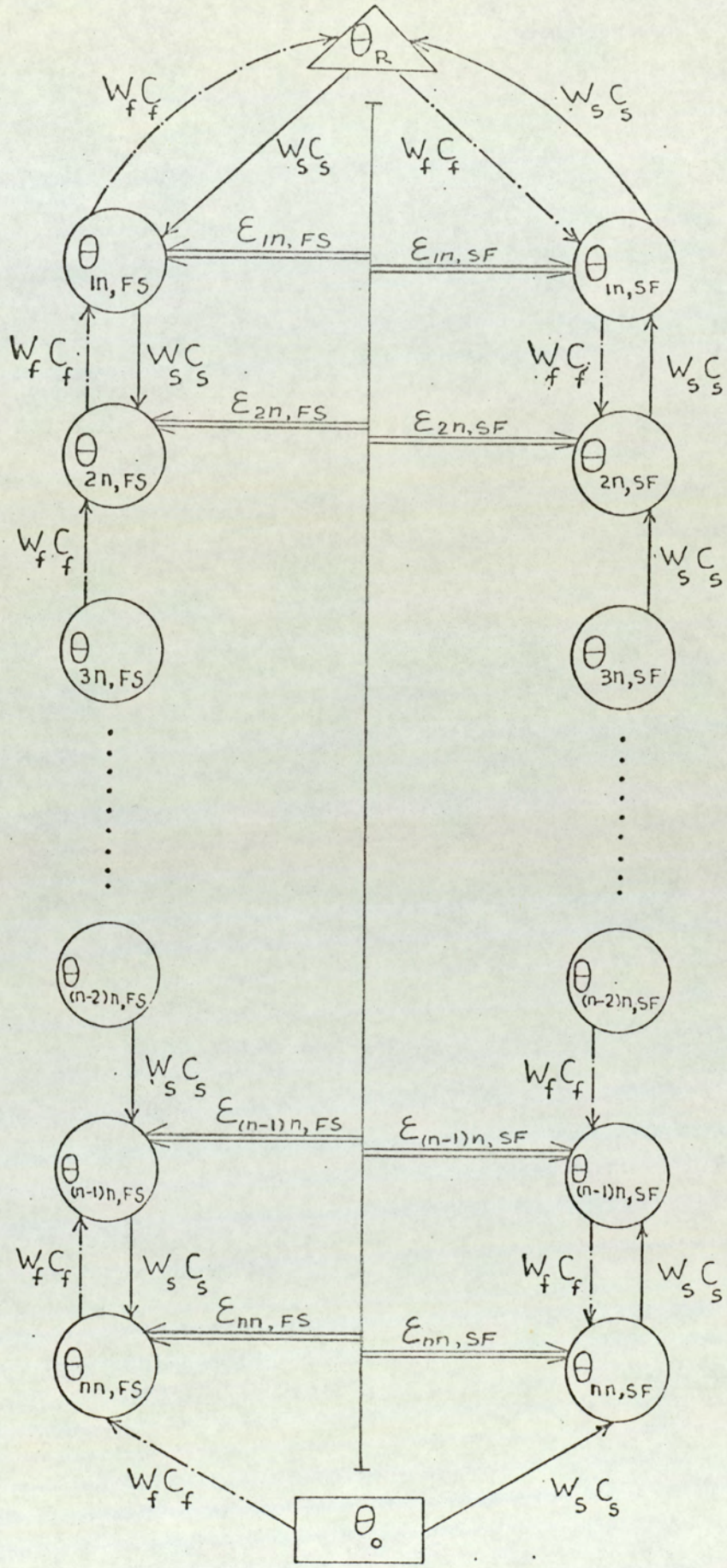

FIG. 5-9: Flow diagram of a lossy fluidised bed process with "n" stages for preheating the fluid and "n" stages for preheating the solid.

5.6. Procedure for the construction and use of the flow diagrams.

1. Write the initial, final and intermediate temperatures enclosed within distinct geometric figures.

2. Use different types of lines to show the different materials and, if helpful, write product of mass and specific heat of the materials near the corresponding lines.

3. Show the temperature change of a particular material by an arrowed line starting from the previous, and ending at the next temperature.

4. An arrow cannot start from a point if it has not reached that point already.

5. If the starting point of an arrow has a lower temperature than the terminal points, then the arrow corresponds to the thermal input; if the situation is reverse, it corresponds to a heat extraction.

6. An arrow starting at a higher temperature may cancel another arrow starting at a lower temperature at the common terminal point. This cancellation corresponds to a heat-balance equation for the materials involved.

7. Uncancelled lines (branches) starting from an initial point and passing through intermediate points before arriving at the terminal point, can be replaced by a single branch between the initial and terminal points. This is illustrated in Figs. 5-7 and 5-8, where branches ($\theta_O \rightarrow \theta_{FS} \rightarrow \theta_R$) in Fig. 5-7 are replaced by branches $\theta_O \rightarrow \theta_R$ in Fig. 5-8. The reverse operation can also be performed.

8. Losses can be considered as explained in section 5-5.

5.7. Conclusions.

New flow diagrams are presented as a practical method for analysing the final temperature states of thermal processes involving heat exchanges between several materials. The method is applicable to many other processes which are governed by balance equations.

The flow diagrams are easy to construct and provide a simple and yet powerful representation of the processes. They also provide conceptual insights into the functionings within such processes, and can also be used for both analysis and design.

6
STEADY STATE ANALYSIS OF FLUIDISED BEDS WITH PREHEATING

6.1. Introduction.

A new approach is presented for quickly analysing the effects of preheating in fluidised beds. It ignores losses, but is a significant facile technique for rapidly estimating the thermal economies resulting from preheating and the effects of extra preheating stages. These estimations are conducted in terms of the thermal properties of the materials in the fluidised bed and the rates of materials handling; thus this method is readily applied to a wide range of fluidised beds. The temperature-equilibrium state of any fluidised bed, irrespective of the number of preheating stages, is conveniently displayed by simple flow diagrams. While fluidised beds are primarily studied, the techniques are equally applicable to other thermal processes involving heat exchange between two materials.

If a process objective is to raise the bed to a desired temperature, this can be achieved by simply heating the fluid before it enters the bed. Then, both the solid particles and the fluidising medium are raised in temperature, compared with their initial temperatures. This permits preheating either material from previously heated material; thus, previously-heated fluid can preheat incoming solid particles, or previously-heated solid particles can preheat incoming fluid. This can reduce the cost of achieving a desired temperature in a process.

This study considers final temperature state conditions in thermal processes. Primary consideration is to processes comprising fluidised beds, heaters, and heat exchangers; although the findings are obviously applicable to many systems involving steady state exchange between two materials at different temperatures. General expressions are derived for the thermal economies achieved by preheating, these economies being identified in terms of the thermal properties of the materials, the rates of materials handling, and the number of preheating stages. These general expressions can be used for the design and analysis of many thermal processes. They extend into a generic form, a recent study of pre-heated fluidised beds[21].

6.2. Fluidised bed.

Figure 5-1 shows a schematic diagram of a fluidised bed system, bed plus heater, without preheating. As it is mentioned in Eq. (5-2),this system can be represented by the flow diagram of Fig. 5-2. It is also stated in Eq. (5-1) that the thermal input to this process is

$$Q_{(\theta_R,\theta_O,O)} = W_f C_f(\theta_R - \theta_O) + W_s C_s(\theta_R - \theta_O) = \frac{k+1}{k} W_s C_s(\theta_R - \theta_O) \qquad (6\text{-}1)$$

where $k = \dfrac{W_s C_s}{W_f C_f}$

and the rest of the symbols are explained in Eq. (5-1).

A process in which the outgoing solid preheats the incoming fluid and the outgoing fluid preheats the incoming solid is considered in the Chapter 5. From Eq. (5-2) the thermal input to this process is

Publication of the results presented in the Ph.D. Thesis:

"Temperature analysis of a class
of electroheated fluidised beds"

by E. Tulunay

The University of Aston in Birmingham, England

September 1969

As on August, 1969.

1. 'Electroheated fluidised beds', Proc. IEE (U.K.), Vol. 116, No. 5, May, 1969, pp. 827 - 833.

2. 'Electrically Indirectly heated fluidised beds', IEEE Trans. Industry and General Applications, (U.S.A.), Accepted for Publication.

   'Fluidised beds with indirect electroheating', Elektrowärme International, (Germany), Accepted for Publication.

3. 'Fluidised beds with preheating', J. Inst. Fuel, (U.K.), Accepted for Publication.

4. 'Modelling a class of electrically-heated fluidised beds used for industrial processes', Conference on "Industrial Application of Dynamic Modelling", University of Durham: 16th-18th September, 1969, IEE Control and Automation Division, (U.K.).

$$Q_{(\theta_R,\theta_O,1F,1S)} = W_f C_f(\theta_R - \theta_{11,FS}) + W_s C_s(\theta_R - \theta_{11,SF})$$
$$= \frac{W_s C_s}{k}(\theta_R - \theta_{11,FS}) + W_s C_s(\theta_k - \theta_{11,SF}) \qquad (6\text{-}2)$$

From Eq. (5-9) the reduction in the thermal input, thermal saving, is

$$Q_{(E,1F,1S)} = W_s C_s(\theta_R - \theta_{11,FS}) + \frac{W_s C_s}{k}(\theta_R - \theta_{11,SF}) \qquad (6\text{-}3)$$

$\theta_{11,SF}$ can be found from heat balance equation. From Eq. (5-4), $\theta_{11,FS}$ is

$$\theta_{11,FS} = \frac{k\theta_R + \theta_O}{k+1} \qquad (6\text{-}4)$$

From Eq. (5-5) $\theta_{11,SF}$ is

$$\theta_{11,SF} = \frac{\theta_R + k\theta_o}{k+1} \qquad (6\text{-}5)$$

6.3. Fluidised bed with "n" stages that preheat fluid.

Consider a process with "n" stages to preheat the fluid by the heated solid. This process is shown as a flow diagram in Fig. 6-1 . From this diagram, the reduction in thermal input is

$$Q_{(E,nF)} = W_s C_s(\theta_R - \theta_{1n,FS}) + W_s C_s(\theta_{1n,FS} - \theta_{2n,FS}) + \ldots$$
$$\ldots + W_s C_s(\theta_{(n-2)n,FS} - \theta_{(n-1)n,FS} + W_s C_s(\theta_{(n-1)n,FS} - \theta_{nn,FS}) \qquad (6\text{-}6)$$
$$= W_s C_s(\theta_R - \theta_{nn,FS})$$

FIG. 6-1

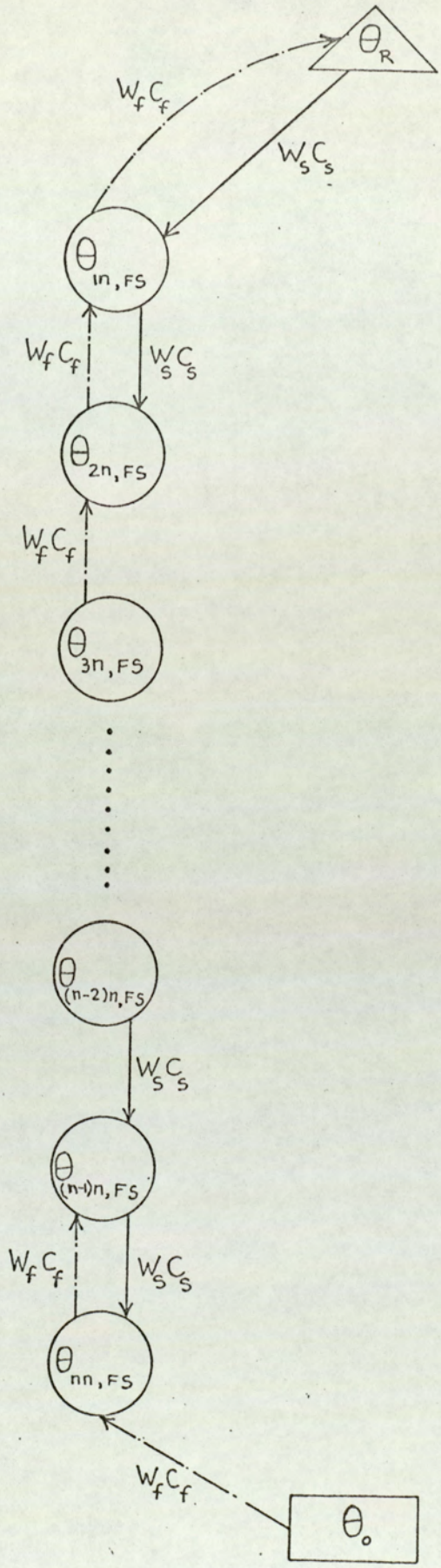

FIG. 6-1: Flow diagram of a fluidised-bed process with "n" stages for preheating the fluid.

It is apparent that the subscripts of $Q_{(E,nF)}$ indicate a reduction (E) in thermal input achieved by n stages to preheat fluid (nF) and no stages to preheat solid. $\theta_{nn,FS}$ is derived from the balance equations as follows

$$
\begin{aligned}
W_s C_s(\theta_R - \theta_{1n,FS}) &= W_f C_f(\theta_{1n,FS} - \theta_{2n,FS}) \\
W_s C_s(\theta_{1n,FS} - \theta_{2n,FS}) &= W_f C_f(\theta_{2n,FS} - \theta_{3n,FS}) \\
W_s C_s(\theta_{2n,FS} - \theta_{3n,FS}) &= W_f C_f(\theta_{3n,FS} - \theta_{4n,FS}) \\
&\vdots \\
W_s C_s(\theta_{(n-2)n,FS} - \theta_{(n-1)n,FS}) &= W_f C_f(\theta_{(n-1)n,FS} - \theta_{nn,FS}) \\
W_s C_s(\theta_{(n-1)n,FS} - \theta_{nn,FS}) &= W_f C_f(\theta_{nn,FS} - \theta_0)
\end{aligned}
\qquad (6\text{-}7)
$$

By arranging the terms we obtain the equation set Eq. (6-8)

$$
\begin{aligned}
-(k+1)\theta_{1n,FS} + \theta_{2n,FS} + 0 + 0 + \ldots + 0 &= -k\theta_R \\
k\theta_{1n,FS} - (k+1)\theta_{2n,FS} + \theta_{3n,FS} + 0 + \ldots + 0 &= 0 \\
0 + k\theta_{2n,FS} - (k+1)\theta_{3n,FS} + 0 + \ldots + 0 &= 0 \\
&\qquad (6\text{-}8) \\
0 + \ldots + 0 + k\theta_{(n-2)n,FS} - (k+1)\theta_{(n-1)n,FS} + \theta_{nn,FS} &= 0 \\
0 + \ldots + 0 + 0 + k\theta_{(n-1)n,FS} - (k+1)\theta_{nn,FS} &= -\theta_0
\end{aligned}
$$

From equation set Eq. (6-8) $\theta_{nn,FS}$ is obtained, (see Appendix B)

$$
\theta_{nn,FS} = \frac{k^n\theta_R + \sum_{i=0}^{i=n-1} k^i\theta_0}{\sum_{i=0}^{i=n} k^i} = \frac{-k^{n+1}\theta_R + k^n(\theta_R - \theta_0) + \theta_0}{-k^{n+1} + 1} \qquad (6\text{-}9)
$$

To obtain the reduction in thermal input, $Q_{(E,nF)}$, substitute $\theta_{nn,FS}$ Eq. (6-9) into Eq. (6-6)

$$Q_{(E,nF)} = W_s C_s \left(\theta_R - \frac{k^n \theta_R + \sum_{i=0}^{i=n-1} k^i \theta_O}{\sum_{i=0}^{i=n} k^i}\right) \qquad (6\text{-}10)$$

$$= W_s C_s \frac{\sum_{i=0}^{i=n-1} k^i (\theta_R - \theta_O)}{\sum_{i=0}^{i=n} k^i}$$

The thermal saving $E_{n,FS}$ can be stated relative to the thermal input with no preheating $Q_{(\theta_R,\theta_O,O)}$ in Eq. (6-1)

$$E_{nF} = \frac{Q_{(E,nF)}}{Q_{(\theta_R,\theta_O,O)}} = \frac{\sum_{i=0}^{i=n-1} k^i}{k+1} \cdot \frac{k}{\sum_{i=0}^{i=n} k^i} \qquad (6\text{-}11)$$

$$= \frac{(k - k^{n+1})}{(1+k)(1-k^{n+1})}$$

6.4. Fluidised bed with "n" stages that preheat solid.

Using the approach of section 6.3., we obtain the expressions for a process with n stages of preheating the solid by the heated fluid. As in Eq. (6-6), the reduction in thermal input will be

$$Q_{(E,nS)} = W_f C_f (\theta_R - \theta_{nn,SF}) \qquad (6\text{-}12)$$

$$\theta_{nn,SF} = \frac{\theta_R + \sum_{i=1}^{i=n} k^i \theta_O}{\sum_{i=0}^{i=n} k^i} \qquad (6\text{-}13)$$

$$= \frac{-k^{n+1}\theta_O - k(\theta_R - \theta_O) + \theta_R}{1 - k^{n+1}}$$

and,

$$E_{nS} = \frac{Q_{(E,nS)}}{Q_{(\theta_R,\theta_O,O)}} = \frac{(k - k^{n+1})}{(1+k)(1-k^{n+1})} = E_{nF} \qquad (6\text{-}14)$$

6.5. Fluidised bed with "n" fluid and "n" solid preheating stages.

Figure 5-5 shows a process with n stages to preheat the fluid with the heated solid and n stages to preheat the solid with the heated fluid. The reduction in thermal input will be

$$\begin{aligned} Q_{(E,nF,nS)} &= W_s C_s(\theta_R - \theta_{1n,FS}) + W_s C_s(\theta_{1n,FS} - \theta_{2n,FS}) + \ldots \\ \ldots &+ W_s C_s(\theta_{(n-2)n,FS} - \theta_{(n-1)n,FS}) + W_s C_s(\theta_{(n-1)n,FS} - \theta_{nn,FS}) \\ &+ W_f C_f(\theta_R - \theta_{1n,SF}) + W_f C_f(\theta_{1n,SF} - \theta_{2n,SF}) + \ldots \\ \ldots &+ W_f C_f(\theta_{(n-2)n,SF} - \theta_{(n-1)n,SF}) + W_f C_f(\theta_{(n-1)n,SF} - \theta_{nn,SF}) \\ &= W_s C_s(\theta_R - \theta_{nn,FS}) + W_f C_f(\theta_R - \theta_{nn,SF}) \\ &= W_s C_s(\theta_R - \theta_{nn,FS}) + \frac{W_s C_s}{k}(\theta_R - \theta_{nn,SF}) \end{aligned} \qquad (6\text{-}15)$$

Using Eqs. (6-9) and (6-13)

$$Q_{(E,nF,nS)} = \frac{2W_s C_s(1 - k^n)}{1 - k^{n+1}}(\theta_R - \theta_o) \qquad (6\text{-}16)$$

FIG. 6-2

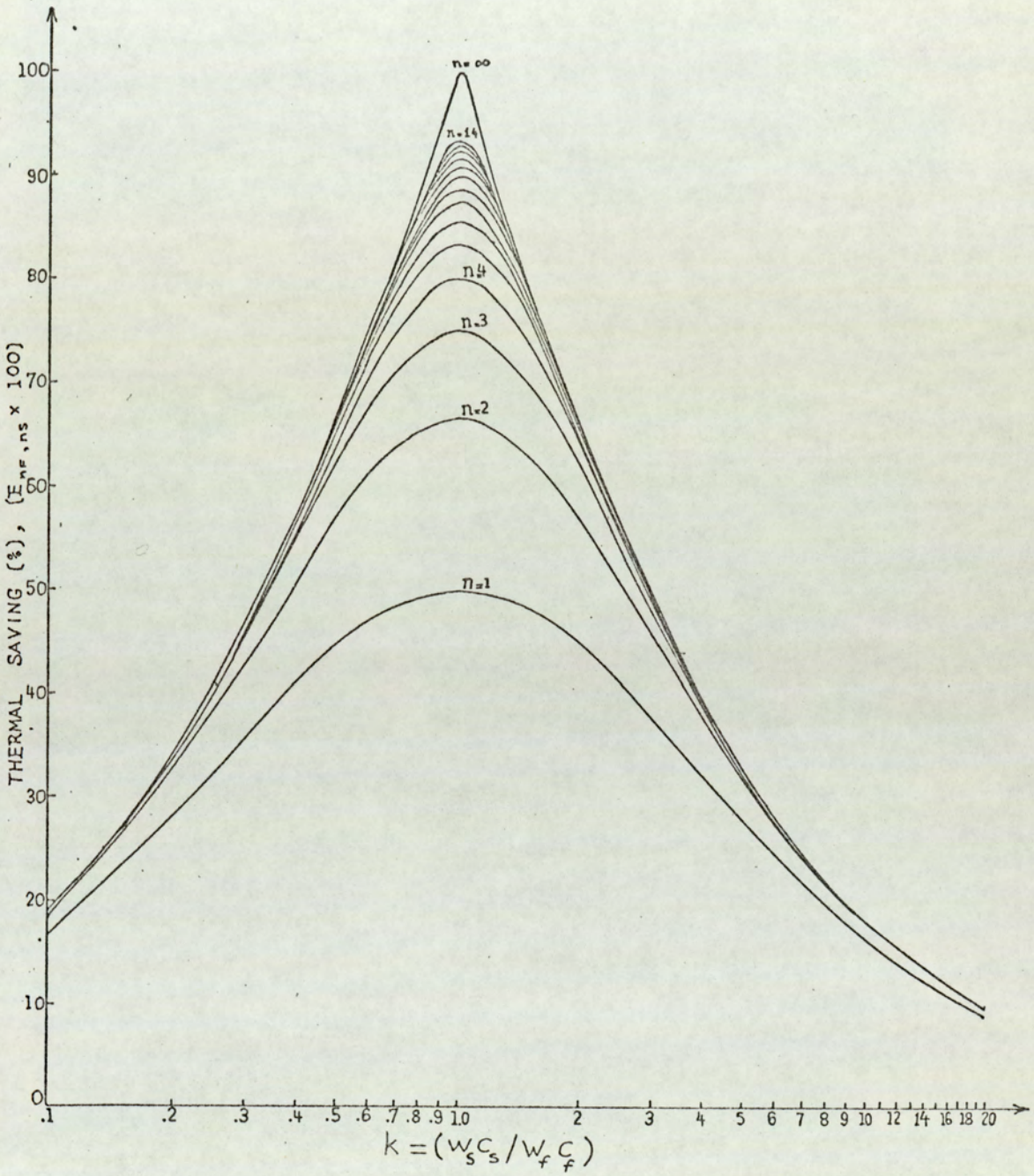

FIG. 6-2: Display of the thermal saving, resulting from preheating, as a function of k and n. The thermal saving is shown as a percentage of the required input without preheating. $k = W_s C_s / W_f C_f$ is an index of the thermal properties of the materials and the materials-handling rate. n is the number of preheating stages.

Dividing $Q_{(E,nF,nS)}$ in Eq. (6-16) by the thermal input for a process without preheating $Q_{(\theta_R,\theta_O,O)}$ in Eq. (6-1) gives the relative saving $E_{nF,nS}$

$$E_{nF,nS} = \frac{Q_{(E,nF,nS)}}{Q_{(\theta_R,\theta_O,O)}} = \frac{2(k - k^{n+1})}{(k+1)(1 - k^{n+1})} = E_{nF} + E_{nS} = 2E_{nF} = 2E_{nS} \qquad (6\text{-}17)$$

In Fig. 6-2 the thermal saving, $E_{nF,nS}$, is displayed as a percentage of the thermal input without preheating, $Q_{(\theta_R,\theta_O,O)}$. The variation of $E_{nF,nS}(\%)$ with k is displayed for different n values. In this display the maxima occur at k = 1. Since from Eq. (6-1)

$$k = \frac{W_s C_s}{W_f C_f}$$

at the maxima

$$W_s C_s = W_f C_f \qquad (6\text{-}18)$$

Equation (6-18) shows that, irrespective of the number of preheating stages, maximum thermal saving is achieved when the solid and the fluid have the same value of (mass) (specific heat)/(unit time). Figure 6-2 together with Eqs. (6-18) and (6-17) are helpful in the design or analysis of thermal processes. As a design example, (6-18) determines the best solid and fluid flow rates (n = given, find k) to obtain maximum thermal saving. As an analysis example, (6-17) determines the thermal economy in a given process (k = given, n = given, find $E_{nF,nS}$). Using Eq. (6-17) or Fig. 6-2 we can construct percent thermal saving ($E_{nS,nF}$ x 100) versus number of preheating stages; n, curves for differing k values (Figs. 6-3 and 4)

FIG. 6-3

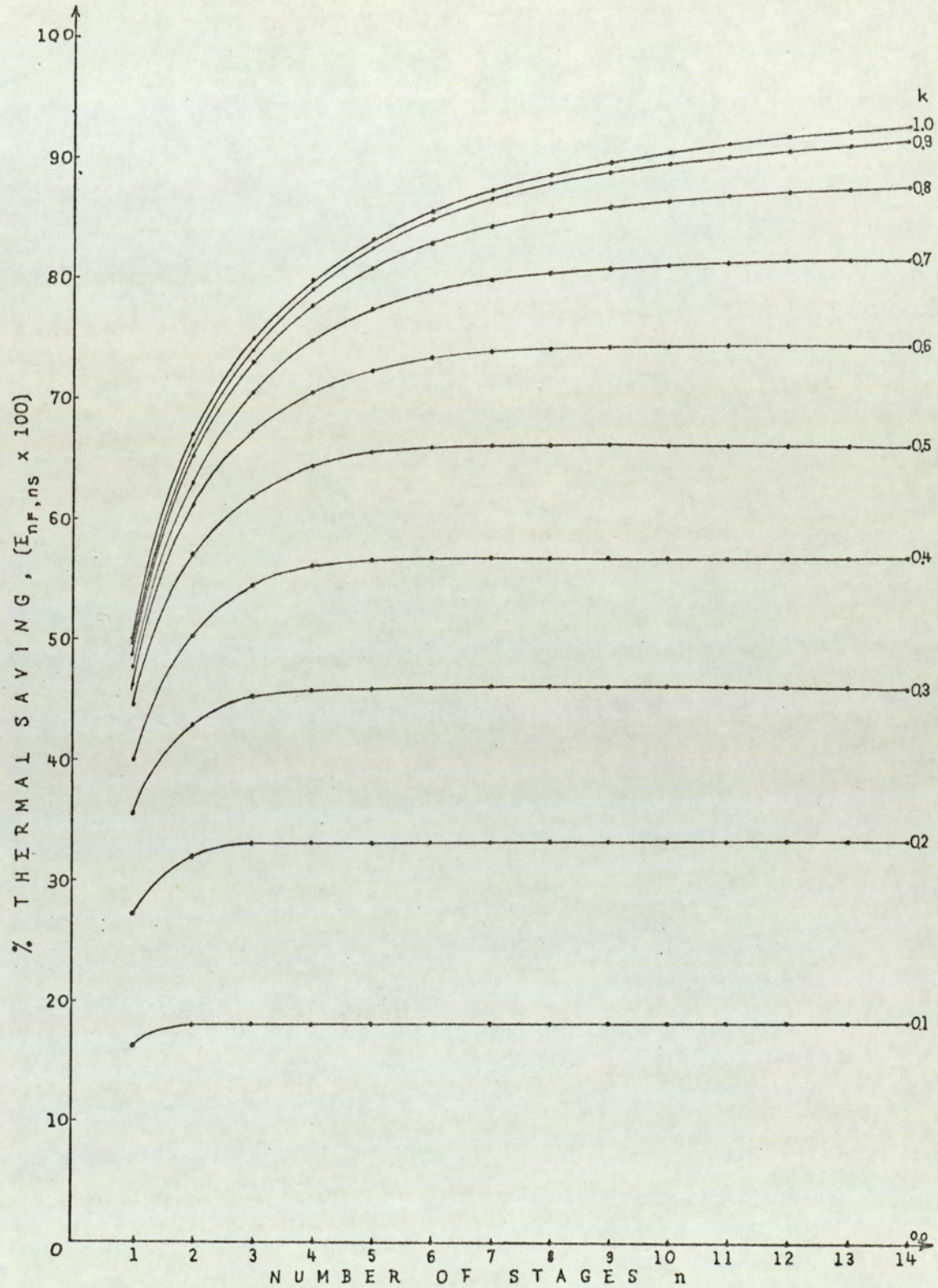

FIG. 6-3: Thermal saving, resulting from preheating, as a a function of n for varying k. Thermal saving is shown as a percentage of the required thermal input without preheating. k is an index of the materials' thermal properties and the materials -handling rates. n is the number of preheating stages. This display is for the range $0 \leq k \leq 1$.

FIG. 6-4

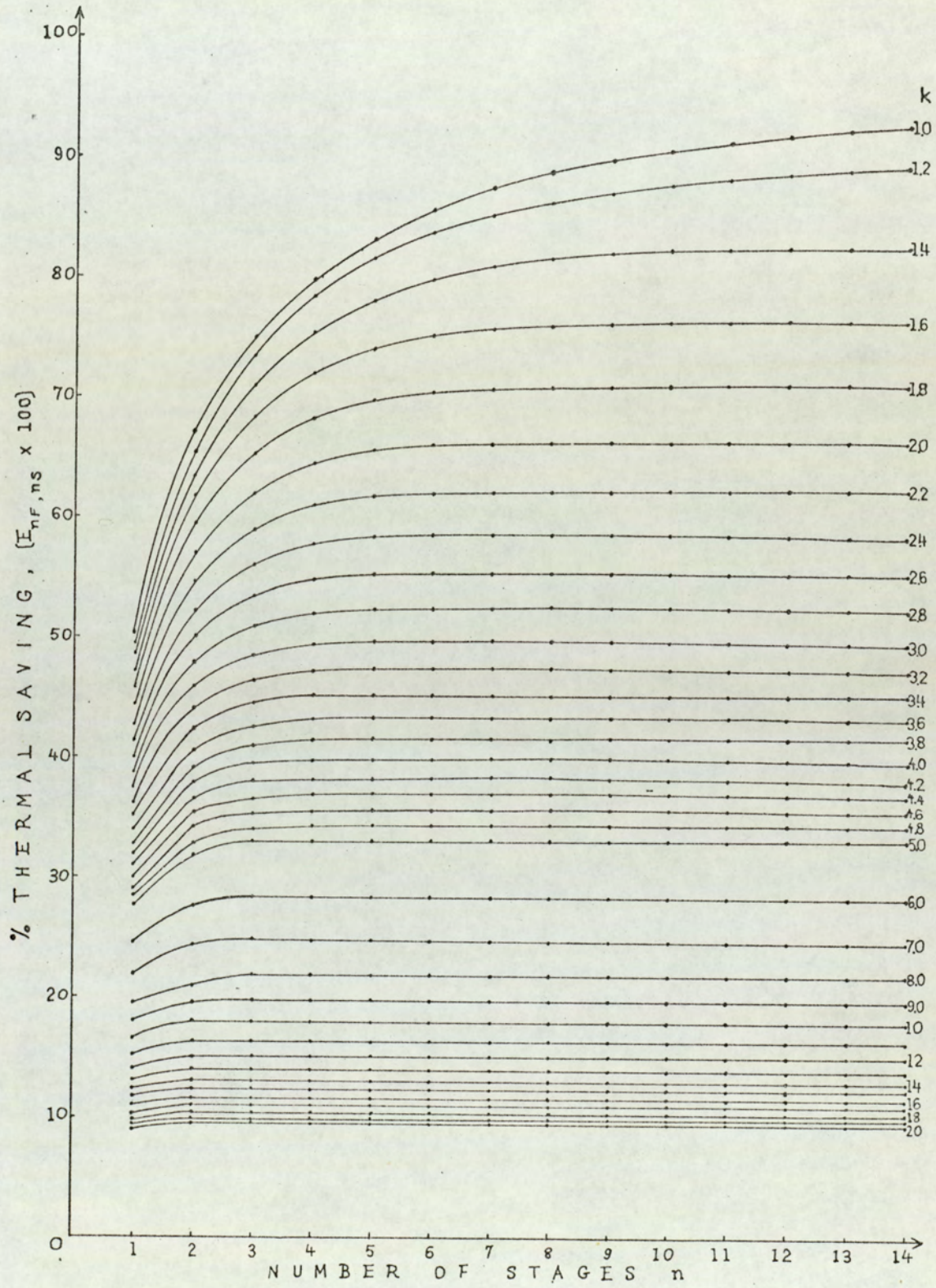

FIG. 6-4: A similar display to Fig. 6-3 but for the range $1 \leq k \leq 20$.

Figures 6-3 and 6-4 can be used to determine the number of preheating stages to obtain a desired thermal saving in a given process ($E_{nS,nF}$ = given, k = given, find n). It is seen that there is a saturation region in these displays. Thus,for a given process there is a practical limit to the savings resulting from the addition of preheating stages.

Applying l'Hospital's rule to Eq. (6-17),

$$\text{Maxima} = \lim_{k \to 1} \frac{2(k - k^{n+1})}{(k+1)(1 - k^{n+1})} = \frac{n}{n+1} \qquad (6\text{-}19)$$

and

$$\lim \frac{2(k - k^{n+1})}{(k+1)(1 - k^{n+1})} \Bigg|_{\substack{k = 1 \\ n \to \infty}} = 1 \qquad (6\text{-}20)$$

As the number of preheating stages increases infinitely, the possible thermal economy approaches the theoretical limit of 100% (provided k is unity). This concept can be checked by considering the limits of $\theta_{nn,FS}$ in Eq. (6-9) and $\theta_{nn,SF}$ in Eq. (6-13)

$$\lim_{\substack{n \to \infty \\ k \geq 1}} \theta_{nn,FS} = \theta_R - \frac{\theta_R - \theta_O}{k} \qquad (6\text{-}21)$$

and

$$\theta_{nn,FS} \Big|_{k = 1} = \theta_O \qquad (6\text{-}22)$$

On the other hand

$$\lim_{\substack{n\to\infty \\ k\geq 1}} \theta_{nn,SF} = \theta_O \quad \text{for all} \quad k \geq 1 \qquad (6\text{-}23)$$

Then by substituting $\theta_{nn,FS}$ and $\theta_{nn,SF}$ values in Eqs. (6-22) and (6-23) in Eq. (6-15) we obtain

$$Q_{(E,nF,nS)}\Big|_{\substack{n\to\infty \\ k=1}} = W_s C_s(\theta_R - \theta_O) + W_f C_f(\theta_R - \theta_O) = Q_{(\theta_R,\theta_O,O)} \qquad (6\text{-}24)$$

and from Eq. (6-17)

$$E_{nF,nS} = \frac{Q_{(E,nF,nS)}}{Q_{(\theta_R,\theta_O,O)}} = 1 \qquad (6\text{-}25)$$

which agrees with Eq. (6-20)

The analysis or design of a process can be conducted for the case of preheated fluid only, or preheated solid only, using Eq. (6-11) or Eq. (6-1 respectively.

Using the equation set (6-8) and similar procedures, the final temperature states $\theta_{in,FS}$ or $\theta_{in,SF}$ of intermediate preheating stages (for which $0 < i < n$) can also be determined.

6.6. Conclusions.

(a) A new general approach has been presented for the analysis and/or design of fluidised beds with preheating heat exchangers. This has resulted from a study of direct and indirect fluidised beds in which a heated solid was used to preheat an incoming fluid, and vice versa.

(b) This is, however, not necessarily restricted to fluidised beds but can be applied to many thermal processes in which heat exchange occurs between two materials at differing temperatures.

(c) Expression for the final temperature states of last preheating stages were derived. Using them, the thermal saving that results from preheating was expressed as a function of the thermal properties of the materials involved, the rates of materials handling and the number of preheating stages. This information was also portrayed as three displays (Figs. 6-2, 6-3 and 6-4).

(d) It was also mentioned that, using the same approach, the final temperature states of intermediate preheating stages can be derived.

(e) The new flow diagrams which are presented in Chapter 5 are used as a practical method for analysing the final temperature states of thermal processes involving heat exchanges between two materials at differing temperatures. They also provide useful conceptual insights into the functions within such processes.

(f) Although the techniques presented take no account of losses, they have been found to be very useful methods for rapidly evaluating economies possible from a proposed arrangement of preheaters, and solving related problems.

7 GENERAL CONCLUSIONS

Individual conclusions of each aspect of this investigation were given at the end of each chapter. Here, the generic conclusions of this investigation are given.

(a) For a class of indirect electroheated fluidised beds, of circular cross-section, with fixed-bed-height/radius ratios in the region of unity, with materials around 60 mesh SiC, sand, etc., new models have been developed for heating and cooling and extended to be flow dependent. These models can be readily established from tests at three flow rates.

(b) For a class of direct electroheated fluidised beds, of circular cross-section, with fixed-bed-height/radius ratios in the region of unity, with material similar to 60-mesh coke, a simplified, modified heating model, and a new cooling model have been developed. These models are flow dependent and can be readily derived by tests at three flow rates.

(c) The curves constructed from these tests provide a facile method for determining the important bed parameters.

(d) New flow diagrams are presented as a practical method for analysing the steady-state temperatures in thermal processes involving heat exchanges between several materials.

(e) A new general approach has been presented by using the new flow diagrams for the analysis and/or design of fluidised beds with preheating heat exchangers. This is, however, not necessarily restricted to fluidised beds but can be applied to many thermal processes involving heat exchange between two materials. Although the techniques take no account of losses, they have been found useful for rapidly evaluating economies possible from a preheating arrangement and calculating the steady state temperatures within the process.

REFERENCES

1. Botterill, J.S.M.: 'Progress in fluidization', British Chemical Engineering, Vol. 10, No. 1, January, 1965, pp. 26-30, and Vol. 13, No. 8, August, 1968, pp. 1121-1126.

2. Hassett, N.J.: 'Developments in applications of fluidization', Chemical and Process Engineering, Vol. 44, No. 3, March, 1963, pp. 127-131.

3. Othmer, D.F.: 'Fluidization', Reinhold, New York, U.S.A., 1956.

4. Leva, N.: 'Fluidization', McGraw-Hill, New York, U.S.A., 1959.

5. Davidson, J.F., Harrison, D.: 'Fluidized Particles', Cambridge University Press, London, G.B., 1963.

6. Motamedi, M., Jameson, G.J.: Shorter communications 'A new method for the measurement of the incipient fluidising velocity', Chem.Engng.Sci., Vol. 23, No. 7, August, 1968, pp. 791-793.

7. Ciborowski, J., Wlodarski, A.: 'On electrostatic effects in fluidised beds', Chem.Engng.Sci. (G.B.), Vol. 17, Jan., 1962, pp. 23-32.

8. Kisel'nikov, V.N., Vyalkov, V.V., Filatov, V.M.: 'On the problem of electrostatic phenomena in a fluidised bed', Int.Chem.Engng., Vol. 7, No. 3, July, 1967, pp. 428-431. (Soviet Union, Khimiya i Khimicheskaya Technologiya, No. 6, 1966, pp. 964-969).

9. Hayakawa, T., Graham, W., Osberg, G.L.: 'A resistance probe method for determining local solid particle mixing rates in a batch fluidised bed', Can.J.Chem.Engng., Vol. 42, June, 1964, pp. 99-103.

10. Goldschmidt, D., Le Goff, P.: 'Electrical methods for the study of a fluidised bed of conducting particles', Trans.Instn.Chem.Engrs., Vol. 45, 1967, pp. T197-T204.

11. Coeuret, F., Le Goff, P.: 'Local porosity, fluctuations of porosity and mass-transfer coefficients in liquid-fluidised beds'. The Chem. Eng., April, 1967, pp. CE75-CE77.

12. Petrenko, I.I., Skvortsov, V.P., Todes, O.M.: 'Express method of determining the quality of fluidisation', Higher Military Tech.Eng. College, Translations from Zavodskaya Laboratoriya, Vol. 33, No.2, Feb., 1967, pp. 188-190.

13. Coeuret, F., Le Goff, P., Vergnes, F.: 'Porosity fluctuations and mass transfer in liquid-fluidised beds', Proc. of the International Symposium on Fluidisation, Editor: A.A.H. Drinkenburg, June, 1967, Eindhoven, pp. 537-552.

14. Goldberger, W.M., Hanway Jr., J.E., Langston, B.G.: 'The electro-thermal fluidised bed', Chem.Engng.Prog., Vol. 61, No. 2, Feb., 1965, pp. 63-67.

15. Johnson, H.S.: 'Reactions in a fluidised coke bed with self-resistive heating', Canadian J. of Chem.Engng., Vol. 39, June, 1961, pp. 145-147.

16. Sevryukov, V.N., Martyushin, I.G.: 'The total electrical resistance of a fluidised bed of electrically conducting granular material', Int.Chem.Engng., Vol. 8, No. 2, April, 1968, pp. 209-211. (Soviet Union, 'Khimicheskaya Promyshlennost' , No. 8, 1967, pp. 46-48.)

17. Graham, W., Harvey, E.A.: 'The electrical resistance of fluidised beds of coke and graphite', Can.J. of Chem.Engng., Vol. 43, June, 1965, pp. 146-149.

18. Reed, A.K., Goldberger, W.M.: 'Electrical behaviour in fluidised beds of conducting solids', Chem.Engng.Symp.Ser., Vol. 62, No. 67, 1966, pp. 71-75.

19. Graham, W., Harvey, E.A., 'The electrical conductivity of fluidised beds of coke and graphite up to 1200°C' Can.J. of Chem.Engng., Vol. 44, February, 1966, pp. 17-19.

20. Goldschmidt, D., Le Goff, P.: Shorter communications 'Résistance électrique des lits fluidisés - I. Résistances moyennes de grains conducteurs fluidisés par air-résultats préliminaires', Chem.Engng.Sci., Vol. 18, 1963, pp. 805-806.

21. Kalinowski, B., Borysowski, J., Wlodarski, R.: 'Heat problems in fluidised bed furnaces', Int.Chem.Engng., Vol. 8, No. 3, July, 1968, pp. 421-426 (Poland, Przemsyl Chemiczny, No. 1, 1968, pp. 30-34).

Appendix A. Description of experimental work

A1. General

The Laboratory models for the study of indirectly and directly-heated fluidised beds are shown in Figs. 3-1 and 4-1 respectively.

The minimum fluidisation point was determined experimentally by using water manometer to monitor the pressure drop across the bed. The experimental curve is shown in Fig. A-1. The defined point of fluidisation is P.

The temperatures at various locations, within the beds were measured by Ni-Cr/Ni-Al thermocouples in conjunction with a Bristol self balancing potentiometric millivolt recorder.

The specifications for each test were as follows:

A1.1. Indirectly-heated bed:

Materials: Silicon carbide 60 mesh

Coke 60 mesh

Flow ranges: 0.2 x 27.6 scfm -

0.35 x 27.6 scfm

Resistance heater energised from AC mains 120W - 300W

Maximum temperature range : 80°C-200°C

A1.2. Directly-heated bed

Material: Coke 60 mesh
(The high resistivity of Silicon Carbide did not permit its use in directly-heated beds).

Flow ranges: 0.2 x 27.6scfm - 0.4 x 27.6 scfm

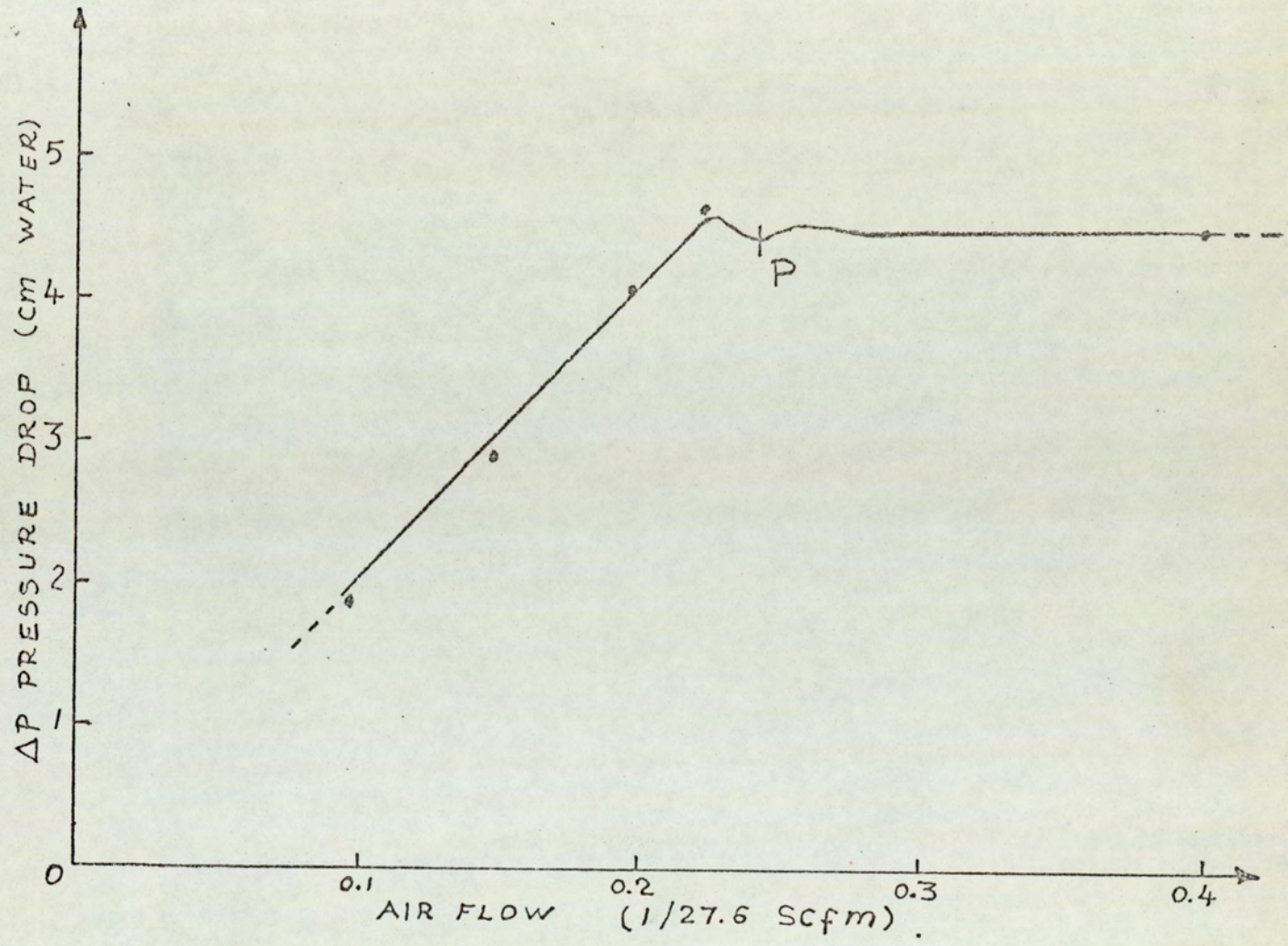

FIG. A-1 : Experimental pressure drop-flow curve

Electrodes: Aluminium strips (see Fig.4-1).

Electrical power: energised from AC mains 80-160 W (evaluated as average of volt x ampere product at various sampled intervals).

Maximum temperature range: 80°C-200°C

Resistance measurement: Averaging out several resistance values measured by Avometer (see Fig. 4-12)

A2. Experimental curves justifying choice of order of process

A2.1 Indirectly-heated fluidised bed

The experimental curves are shown in Figs. A-2, A-3 and A4 to justify the arguments on page 9.

On these curves the scale for the horizontal axis is 1.67min/div. and the vertical axis 1mv/div.

Figure A-2 shows the heating and cooling curves for very high flow f3 at which the bed behaves like a first order system. For this figure:

Material SiC 60 mesh

Flow Rate 0.38 x 27.6 scfm

Electrical power 169 W

Figure A-3 shows the heating and cooling curves for low flow. For this figure:

Material SiC 60 mesh

Flow Rate 0.23 x 27.6 scfm

Electrical power 250 W

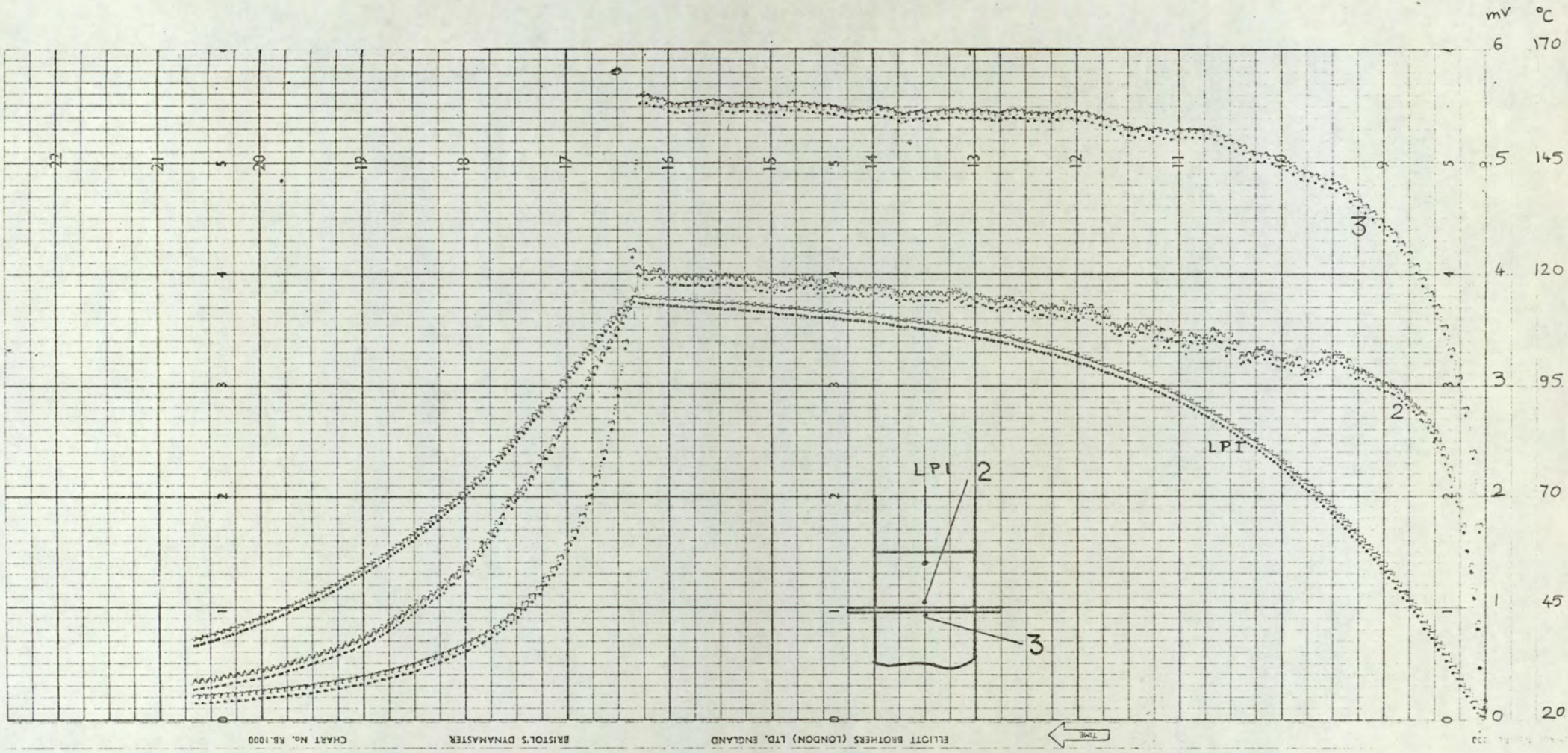

FIG. A-2: Heating and cooling curves of the indirectly-heated bed at very high flow f_3 (f_3 = 0.38 x 27.6 scfm).

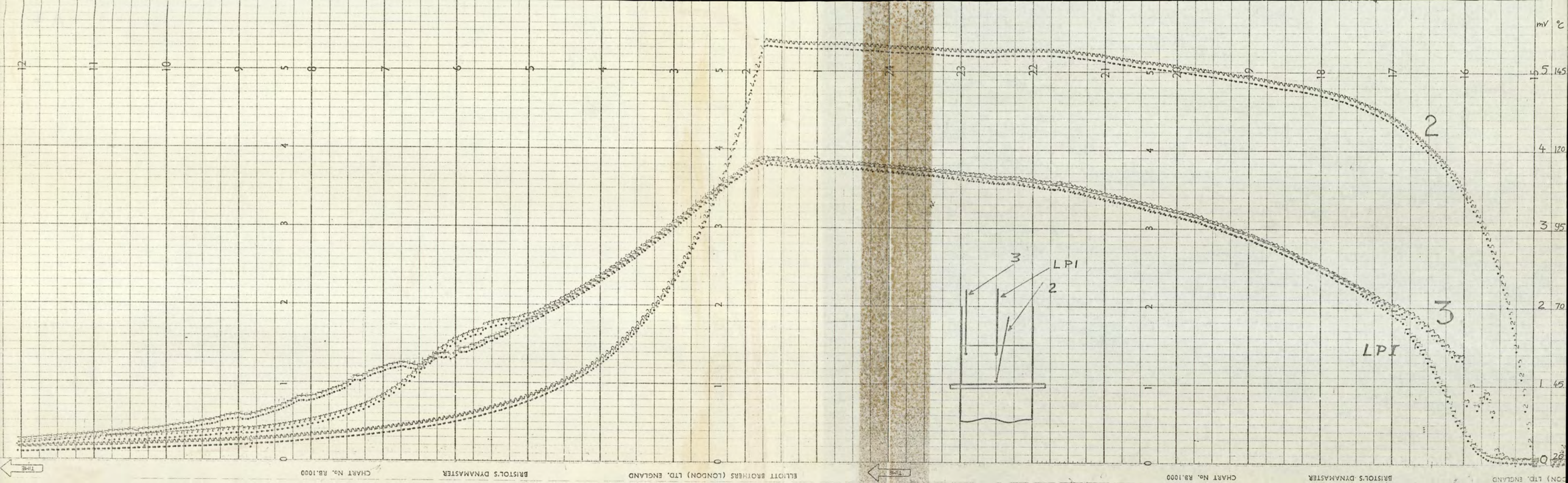

FIG. A-3: Heating and cooling curves of the indirectly-heated bed at low flow.

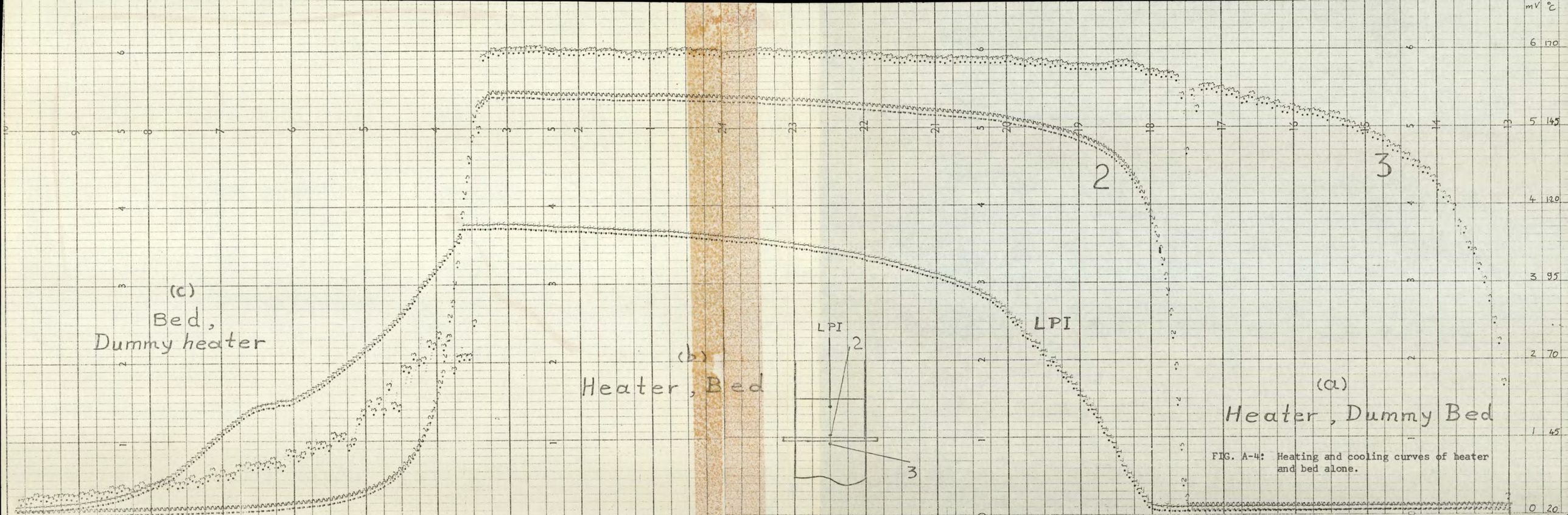

FIG. A-4: Heating and cooling curves of heater and bed alone.

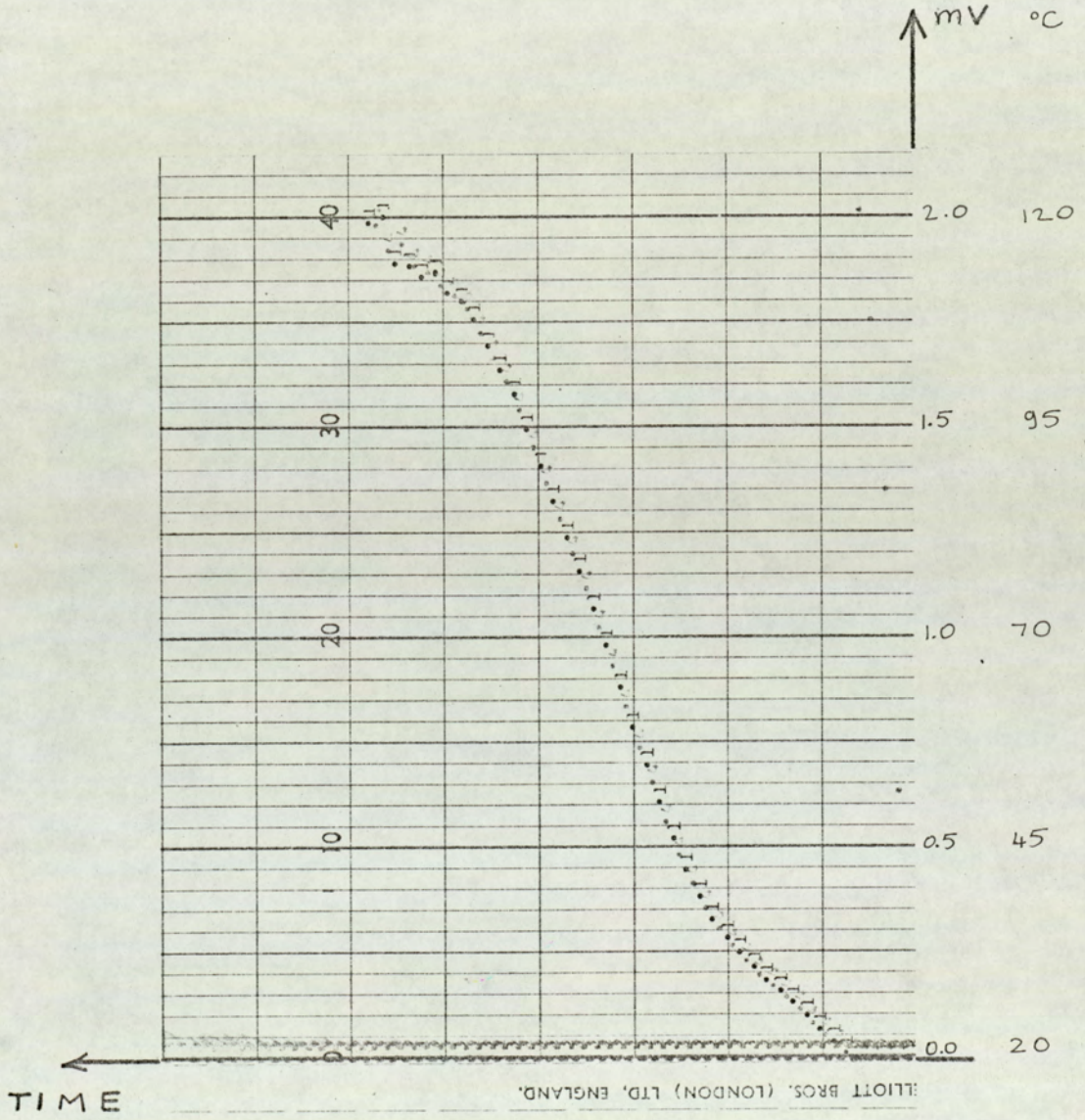

FIG. A-5 : Heating curve for coke

Fig. A-4 shows the heating and cooling curves for

a) Heater + dummy bed

b) Heater + bed

c) Dummy heater + bed (cooling)

For this figure

Material SiC 60 mesh

Flow Rate 0.23 x 27.6 scfm

Electrical power 250 W

Time delay is observed at the beginning of the curves.

Fig. A-5 shows the heating curve for 60 mesh coke particles.

For this figure

Horizontal scale: 1.67 div./min

Vertical scale: 0.5 mv/div.

Material: Coke 60 mesh

Flow Rate: 0.22 x 27.6 scfm

Electrical power: 250 W

A2.2. Directly-heated fluidised bed

Experimental curves for the directly-heated bed are shown in Figs. A-6 - A-9.

On these curves the scale for the horizontal axis is 1.67min/div and for the vertical axis is 1 mv/div. respectively.

Figures A-6 and A-7 show the heating curves for low and high flows respectively.

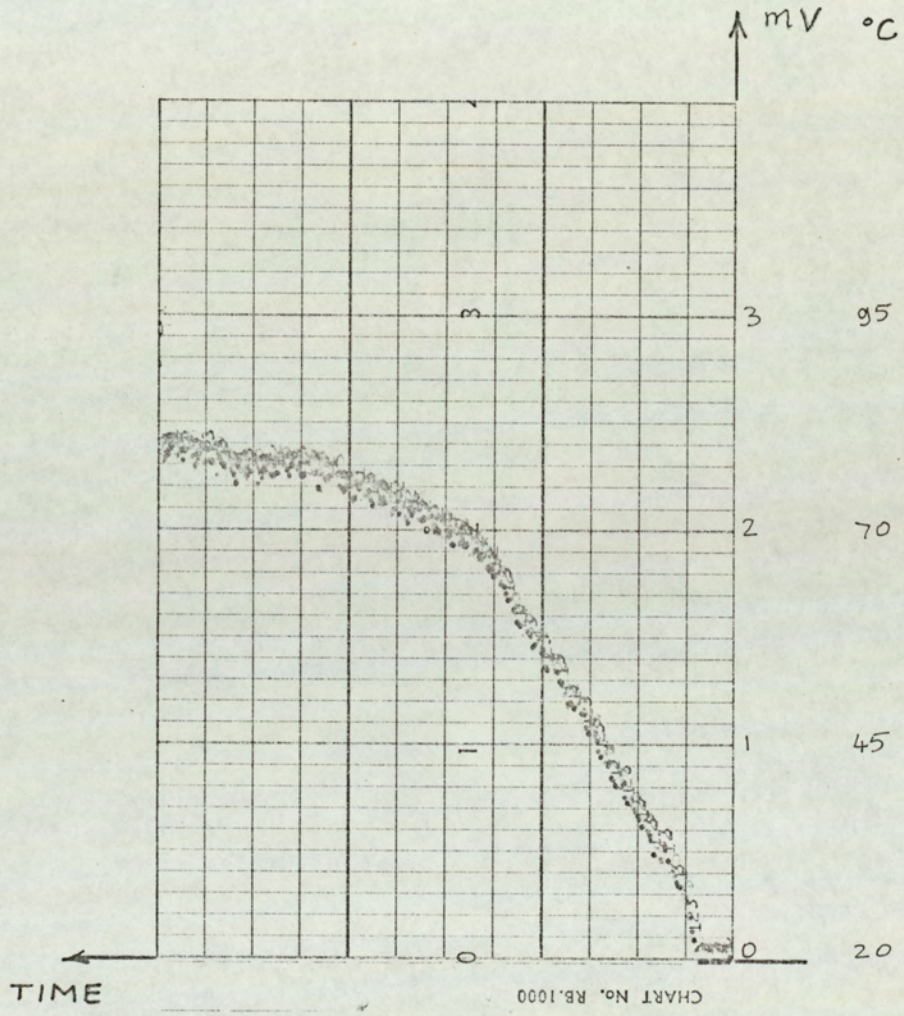

FIG. A-6 : Heating curve of the directly-heated bed at low flow

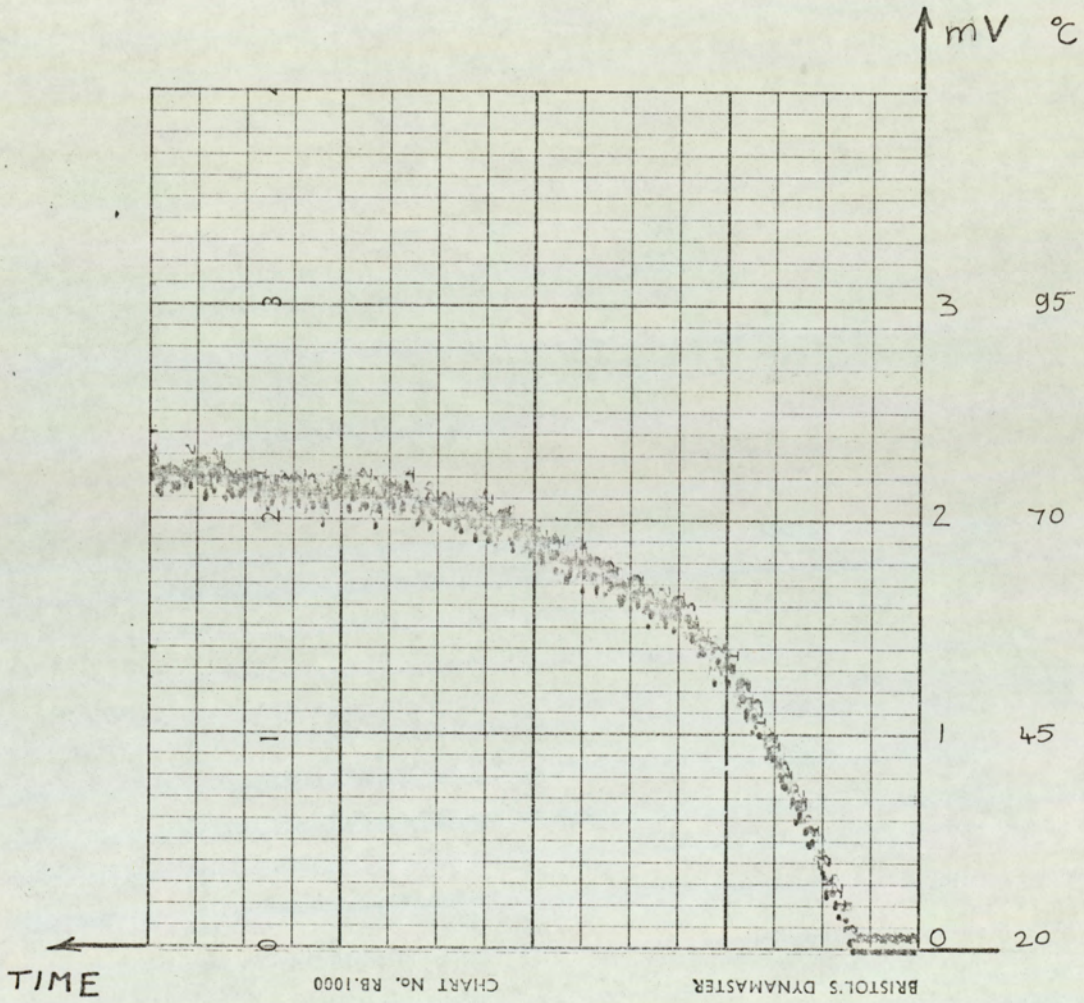

FIG. A-7 : Heating curve of the directly-heated bed at high flow

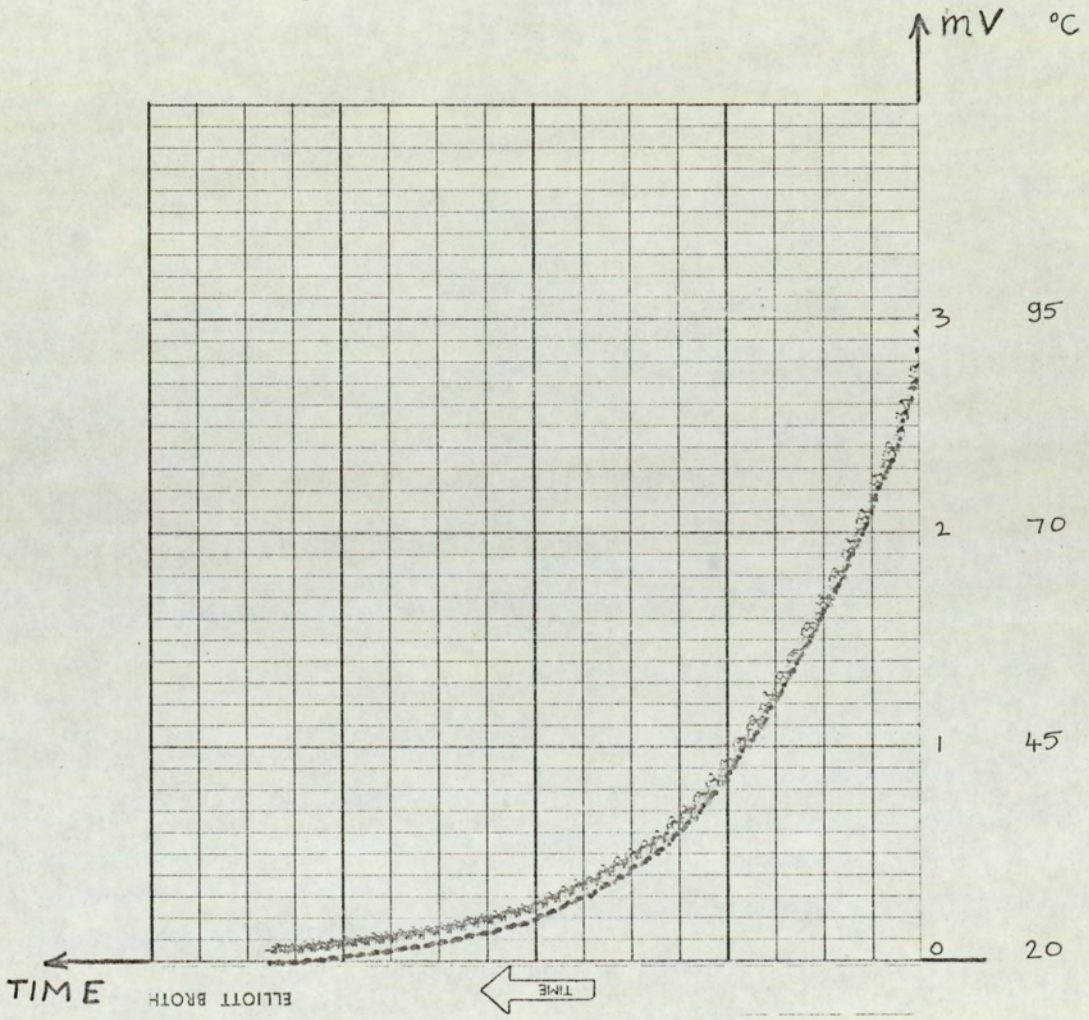

FIG. A-8 : Cooling curve of the directly-heated bed at high flow.

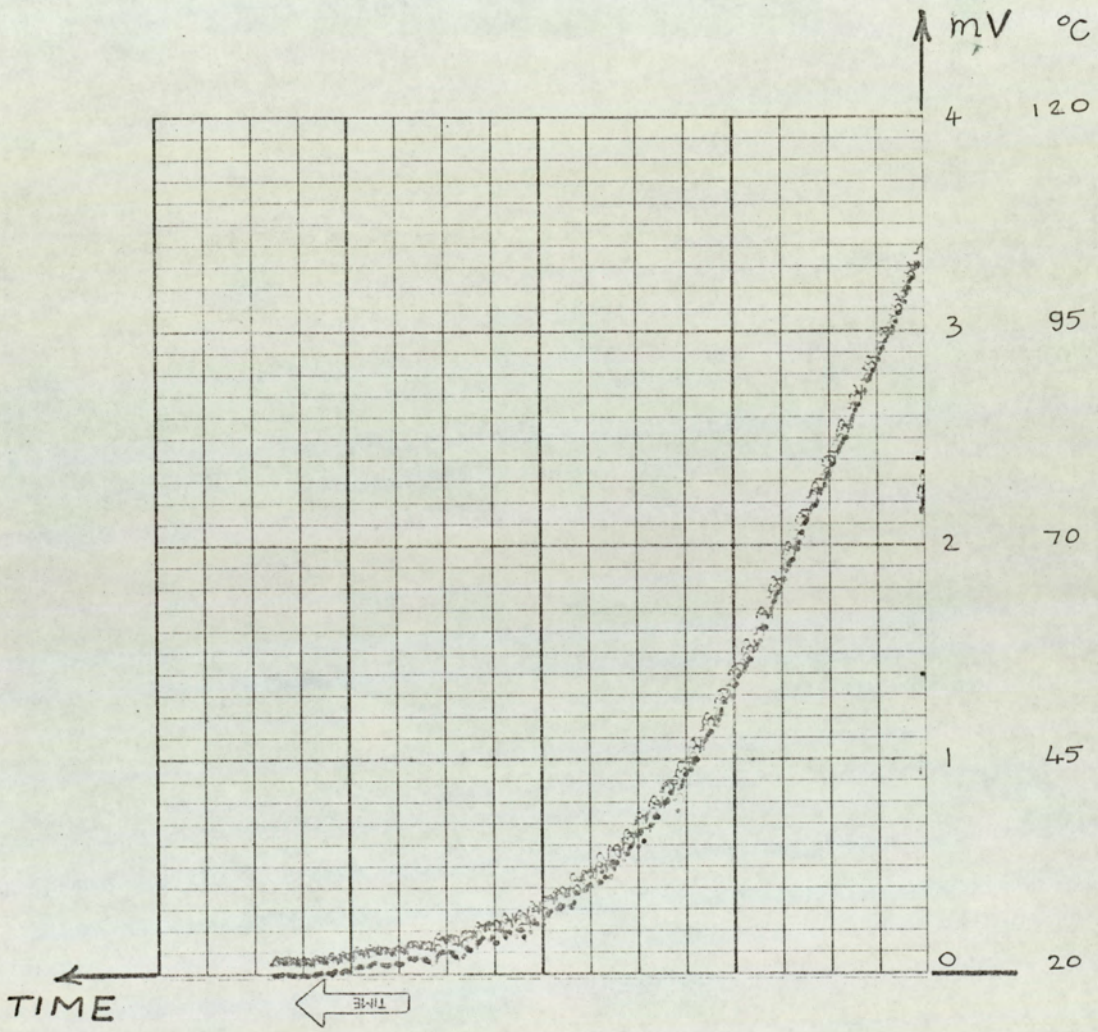

FIG. A-9 : Cooling curve of the directly-heated bed at low flow.

For Figure A-6:

Material: Coke 60 mesh

Flow Rate: 0.25 x 27.6 scfm

Electrical power 120 W

For Figure A-7:

Material: Coke 60 mesh

Flow Rate: 0.3 x 27.6 scfm

Electrical power 160W

Figures A-8 and A-9 show the cooling curves:

For Figure A-8

Material: Coke 60 mesh

Flow Rate: 0.35 x 27.6 scfm

For Figure A-9

Material: Coke 60 mesh

Flow Rate: 0.3 x 27.6 scfm

A.3. Resistance and power measurements

Average resistance measurements are shown in Fig. A-10 graphically for the operating conditions specified in section A1.2.

Actual power measurement values are tabulated in Table A-1.

V	Volt	105	105	105	105
I	Ampere	0.9	0.8	0.85	0.85
P_i	watt	94.5	84.0	89.25	89.25

Flow = 0.3 x 27.6

$$\text{Average power} = \frac{\sum_{i=1}^{n} P_i}{n} = \frac{357.5}{4} = 89.37 \text{ W}$$

Table A-1: Actual power values.

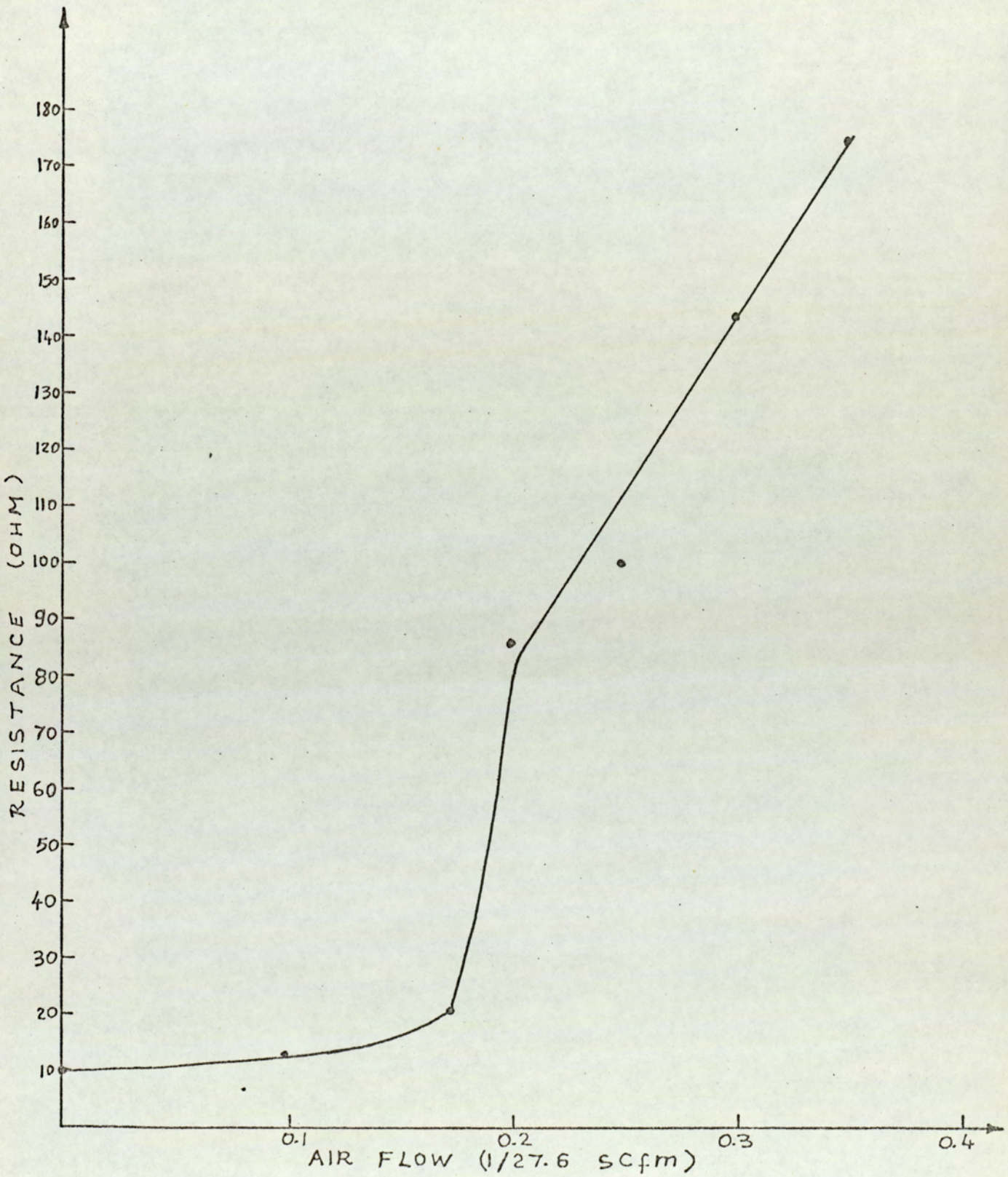

FIG. A-10 : Average resistance - flow graph.

A4. Conclusions

Although these experimental results are confined to the conditions specified, the general arguments may be applied equally well for processes operating under extended conditions provided the output responses are of the same form.

APPENDIX B. The calculation of $\theta_{nn,FS}$ in Chapter 6

From the equation set of Eq.(6-8) by Cramer's rule

$$\theta_{nn,FS} = \frac{D_{nn,FS}}{\Delta_{nn,FS}} \qquad (B\text{-}1)$$

where $\Delta_{nn,FS}$ is the n x n system determinant

$D_{nn,FS}$ is the determinant formed by replacing the nth column in $\Delta_{nn,FS}$ by the right hand side of the equations in (6-8)

To evaluate the determinants $D_{nn,FS}$ and $\Delta_{nn,FS}$, the mathematical induction method is used:

take $\Delta_{nn,FS}$. After solving the equation set (6-8) for n = 0, 1, 2, 3 assume that for n = (r-1) the determinant is

$$\Delta_{(r-1)(r-1),FS} = (-1)^{r-1} \sum_{i=0}^{i=r-1} k^i \qquad (B\text{-}2)$$

Now, take n = r,

$$\Delta_{rr,FS} = \begin{vmatrix} -(k+1) & 1 & 0 & 0.....0 & 0 & 0 \\ k & -(k+1) & 1 & 0.....0 & 0 & 0 \\ 0 & k & -(k+1) & 1.....0 & 0 & 0 \\ \cdot & \cdot & \cdot & \cdot \quad \cdot & \cdot & \cdot \\ \cdot & \cdot & \cdot & \cdot \quad \cdot & \cdot & \cdot \\ \cdot & \cdot & \cdot & \cdot \quad \cdot & \cdot & \cdot \\ 0 & 0 & 0 & 0.....k & -(k+1) & 1 \\ 0 & 0 & 0 & 0.....0 & k & -(k+1) \end{vmatrix} \qquad (B\text{-}3)$$

and

$$\Delta_{rr,FS} = -(k+1)\Delta_{(r-1)(r-1),FS} - \begin{vmatrix} k & 1 & 0 & 0 & 0 & 0 \\ 0 & -(k+1) & 1 & 0 & 0 & 0 \\ \cdot & \cdot & \cdot & \cdot & \cdot & \cdot \\ \cdot & \cdot & \cdot & \cdot & \cdot & \cdot \\ \cdot & \cdot & \cdot & \cdot & \cdot & \cdot \\ 0 & 0 & 0 & 0 & k & -(k+1) \end{vmatrix}$$

$$= -(k+1)\Delta_{(r-1)(r-1),FS} - k\Delta_{(r-2)(r-2),FS} \qquad \text{(B-4)}$$

Since $r-2<r-1$ for $n = r-2$, the assumption of Eq. (B-2) can also be used. Then,

$$\Delta_{rr,FS} = -(k+1)(-1)^{(r-1)} \sum_{i=0}^{i=r-1} k^i - k(-1)^{(r-2)} \sum_{i=0}^{i=r-2} k^i$$

$$= (-1)^r \sum_{i=1}^{i=r} k^i + (-1)^r \sum_{i=0}^{i=r-1} k^i + (-1)^{(r-1)} \sum_{i=1}^{i=r-1} \qquad \text{(B-5)}$$

$$= (-1)^r \sum_{i=0}^{i=r} k^i$$

So, the assumption of Eq. (B-2) is proved to be true for $n = r$. Then, in general

$$\Delta_{nn,FS} = (-1)^n \sum_{i=0}^{i=n} k^i \qquad \text{(B-6)}$$

Similarly, repeating the same procedure,

$$D_{(r-1)(r-1),FS} = k^{r-1}\theta_R + \sum_{i=0}^{i=r-1} k^i\theta_0 \qquad \text{(B-7)}$$

$$D_{rr,FS} = \begin{vmatrix} -(k+1) & 1 & 0 & 0 & 0 & 0 & -k\theta_r \\ k & -(k+1) & 1 & 0 & 0 & 0 & 0 \\ 0 & k & -(k+1) & 1 & 0 & 0 & 0 \\ \cdot & \cdot & \cdot & \cdot & \cdot & \cdot & \cdot \\ \cdot & \cdot & \cdot & \cdot & \cdot & \cdot & \cdot \\ \cdot & \cdot & \cdot & \cdot & \cdot & \cdot & \cdot \\ 0 & 0 & 0 & 0 & k & -(k+1) & 0 \\ 0 & 0 & 0 & 0 & 0 & k & -\theta_0 \end{vmatrix} \qquad \text{(B-8)}$$

$$= (-1)^r(-k\theta_r) \begin{vmatrix} k & -(k+1) & 1 & 0.....0 \\ 0 & k & -(k+1) & 0.....0 \\ \cdot & \cdot & \cdot & \cdot \\ \cdot & \cdot & \cdot & \cdot \\ \cdot & \cdot & \cdot & \cdot \\ 0 & 0 & 0 & 0.....k \end{vmatrix} - \theta_0 \, \Delta_{(r-1)(r-1),FS} \qquad \text{(B-9)}$$

Using Eq. (B-6),

$$D_{rr,FS} = (-1)^r (-k\theta_R) k^{r-1} - \theta_0 (-1)^{r-1} \sum_{i=0}^{r-1} k^i$$

and, (B-10)

$$D_{rr,FS} = (-1)^r \left[k^r \theta_R + \sum_{i=0}^{i=r-1} k^i \theta_0 \right]$$

Then, in general

$$D_{nn,FS} = (-1)^n \left[k^n \theta_R + \sum_{i=0}^{i=n-1} k^i \theta_0 \right] \qquad \text{(B-11)}$$

Thus, from Eq.(B-1) $\theta_{nn,FS}$ is

$$\theta_{nn,FS} = \frac{k^n \theta_R + \sum_{i=0}^{i=n-1} k^i \theta_0}{\sum_{i=0}^{i=n} k^i} \qquad \text{(B-12)}$$